

Magnetic phase diagram of the spin-1/2 antiferromagnetic zigzag ladder

T. Hikihara,¹ T. Momoi,² A. Furusaki,² and H. Kawamura³

¹*Department of Physics, Hokkaido University, Sapporo 060-0810, Japan*

²*Condensed Matter Theory Laboratory, RIKEN, Wako, Saitama 351-0198, Japan*

³*Department of Earth and Space Science, Faculty of Science, Osaka University, Toyonaka 560-0043, Japan*

(Dated: May 31, 2019)

We study the one-dimensional spin-1/2 Heisenberg model with antiferromagnetic nearest-neighbor J_1 and next-nearest-neighbor J_2 exchange couplings in magnetic field h . With varying dimensionless parameters J_2/J_1 and h/J_1 , the ground state of the model exhibits several phases including three gapped phases (dimer, 1/3-magnetization plateau, and fully polarized phases) and four types of gapless Tomonaga-Luttinger liquid (TLL) phases which we dub TLL1, TLL2, spin-density-wave (SDW₂), and vector chiral phases. From extensive numerical calculations using the density-matrix renormalization-group method, we investigate various (multiple-)spin correlation functions in detail, and determine dominant and subleading correlations in each phase. For the one-component TLLs, i.e., the TLL1, SDW₂, and vector chiral phases, we fit the numerically obtained correlation functions to those calculated from effective low-energy theories of TLLs, and find good agreement between them. The low-energy theory for each critical TLL phase is thus identified, together with TLL parameters which control the exponents of power-law decaying correlation functions. For the TLL2 phase, we develop an effective low-energy theory of two-component TLL consisting of two free bosons (central charge $c = 1 + 1$), which explains numerical results of entanglement entropy and Friedel oscillations of local magnetization. Implications of our results to possible magnetic phase transitions in real quasi-one-dimensional compounds are also discussed.

PACS numbers: 75.10.Jm, 75.10.Pq, 75.40.Cx

I. INTRODUCTION

Frustrated quantum antiferromagnets have long been a subject of active research, since Anderson¹ suggested resonating-valence-bond (RVB) ground state for a triangular lattice antiferromagnet. Recent experimental studies of quasi-two-dimensional compounds, such as the organic Mott insulator² κ -(BEDT-TTF)₂Cu₂(CN)₃ and the transition metal chloride Cs₂CuCl₄,³ have further prompted theoretical research of anisotropic triangular lattice antiferromagnets.^{4–11} In these anisotropic quasi-two-dimensional antiferromagnets combination of frustrated exchange interactions and strong quantum fluctuations suppresses tendency toward conventional magnetic orders, thereby opening up possibilities of exotic quantum states.

A zigzag spin ladder is a one-dimensional (1D) strip of the anisotropic triangular lattice spin system, and can be regarded as a minimal, toy model of (strongly anisotropic quasi-two-dimensional) frustrated quantum magnets. Furthermore, the 1D J_1 - J_2 Heisenberg model on the zigzag ladder is in itself a good model for various quasi-1D magnetic compounds, such as (N₂H₅)CuCl₃,^{12–14} Rb₂Cu₂Mo₃O₁₂,¹⁵ and LiCuVO₄.^{16–20} Despite its simplicity, the 1D J_1 - J_2 Heisenberg model has been shown to exhibit various unconventional phases under magnetic field (as we summarize below).^{21–24} In this paper we aim to clarify the nature of the phases in the ground-state phase diagram of the 1D spin-1/2 J_1 - J_2 Heisenberg model under magnetic field, when both the nearest- and next-nearest-neighbor exchange couplings are *antiferromagnetic* (AF). To this end, we study in detail spin

correlations in each phase using the numerical density matrix renormalization group (DMRG) method as well as low-energy effective theory based on bosonization.

The Hamiltonian of the J_1 - J_2 Heisenberg spin chain is given by

$$\mathcal{H} = J_1 \sum_l \mathbf{s}_l \cdot \mathbf{s}_{l+1} + J_2 \sum_l \mathbf{s}_l \cdot \mathbf{s}_{l+2} - h \sum_l s_l^z, \quad (1)$$

where \mathbf{s}_l is a spin-1/2 operator at l th site, J_1 and J_2 are respectively the nearest- and next-nearest-neighbor exchange couplings ($J_1 > 0$ and $J_2 > 0$), and h is external magnetic field along the z -direction.

In the classical limit, the ground state of the zigzag ladder J_1 - J_2 Heisenberg antiferromagnet has a helical magnetic structure

$$\mathbf{s}_l = s(\sin \theta^c \cos \phi_l^c, \sin \theta^c \sin \phi_l^c, \cos \theta^c) \quad (2)$$

with a pitch angle

$$\phi^c = \phi_{l+1}^c - \phi_l^c = \pm \arccos \left(\frac{-J_1}{4J_2} \right) \quad (3)$$

and a canting angle

$$\theta^c = \arccos \left(\frac{4hJ_2}{s(J_1 + 4J_2)^2} \right) \quad (4)$$

for $J_2/J_1 > 1/4$, whereas the ground state has canted Néel order for $J_2/J_1 \leq 1/4$.

In the quantum ($s = 1/2$) case, the ground-state properties of the model (1) change drastically from the classical spin state. The ground state at zero magnetic field $h = 0$ has been understood quite well. For

small $J_2/J_1 < (J_2/J_1)_c$, the ground state is in a critical Tomonaga-Luttinger liquid (TLL) phase with gapless excitations. The model undergoes a quantum phase transition at $(J_2/J_1)_c = 0.2411$,^{29–31} to a gapped phase with spontaneous dimerization^{25–28} for $J_2/J_1 > (J_2/J_1)_c$. It is also known that the model exhibits a long-range order (LRO) of vector chirality in the case of anisotropic exchange couplings.^{32–34}

With applied magnetic field, the phase diagram becomes even richer. From numerical studies of the magnetization process, it has been found that for a certain range of J_2/J_1 the magnetization curve exhibits a plateau at one-third of the saturated magnetization and cusp singularities.^{21,35–37} In this 1/3-plateau phase, the ground state has a magnetic LRO of *up-up-down* structure. Furthermore, it was found that away from the 1/3-plateau and at $J_2/J_1 \gtrsim 1$, the total magnetization $S_{\text{tot}}^z = \sum_l s_l^z$ changes in units of $\Delta S_{\text{tot}}^z = 2$, indicating that two spins form a bound pair and flip simultaneously as the field h increases.^{21,36} These characteristic changes in the magnetization process give accurate estimates of phase boundaries, which divide the parameter space into several regions (see Fig. 1 below), although the magnetization process alone cannot give much information on the nature of each phase.

Another interesting feature of the J_1 - J_2 chain in magnetic field is a field-induced LRO of the vector chirality,

$$\kappa_l^{(n)} = (\mathbf{s}_l \times \mathbf{s}_{l+n})^z. \quad (5)$$

In zero field, the vector chiral LRO has been found when and only when the system has an easy-plane anisotropy.^{32–34,38,39} In this case, due to the anisotropy, symmetry of the system in spin space is lowered from isotropic $SU(2)$ to $U(1) \times Z_2$, where the $U(1)$ and Z_2 symmetries correspond to the rotation in the easy plane and the sign of pitch angle of helical spin order, respectively. While the continuous $U(1)$ symmetry is preserved in the quantum case $s = |s| < \infty$,⁴⁰ the discrete Z_2 symmetry can be spontaneously broken even in the quantum limit $s = 1/2$, thereby resulting in the vector chiral phase. This line of symmetry consideration suggests that the magnetic field, which induces the same symmetry reduction, should also lead to the spontaneous symmetry breaking of the Z_2 symmetry. Indeed, this possibility was first pointed out by Kolezhuk and Vekua,⁴¹ who have predicted from a field-theoretical analysis that the vector chiral LRO may set in for a large J_2/J_1 regime. Recently, the appearance of the vector chiral LRO under magnetic field was verified numerically.^{42,43}

In this paper, we report our numerical and analytic results of the ground-state properties in the various phases that appear under magnetic field. From a thorough comparison of long-distance behavior of correlation functions, we identify effective theories that describe the low-energy physics of each phase. For this purpose, we calculate numerically various correlation functions, which include longitudinal-spin, transverse-spin, vector chiral, and nematic (two-magnon) correlation functions using

the DMRG method.^{44,45} Comparing the numerical results with asymptotic forms derived from bosonization analysis, we find that, in addition to the gapped dimer phase, 1/3-plateau phase, and ferromagnetic phase, the system exhibits four critical phases: (i) a phase with one-component TLL which is adiabatically connected to the ground state of the 1D Heisenberg antiferromagnet (TLL1 phase), (ii) a two-component TLL phase (TLL2 phase), (iii) a vector chiral phase, and (iv) a spin-density-wave phase with two-spin bound pairs (SDW₂ phase). The low-energy states in the TLL1, vector chiral, and SDW₂ phases turn out to be one-component TLLs (a conformal field theory with central charge $c = 1$). Furthermore, we estimate the TLL parameter for the one-component TLL phases as a function of J_2/J_1 and the magnetization. Since the TLL parameter governs asymptotic behaviors of correlation functions, it has direct relevance to various experimental observables such as a magnetic LRO emerging in real quasi-1D compounds with weak interchain couplings and temperature dependence of relaxation rates ($1/T_1$) in nuclear magnetic resonance experiments.^{46,47}

This paper is organized as follows: In Sec. II, we show the ground-state phase diagram under magnetic field (see Fig. 1), which contains the TLL1, 1/3-plateau, SDW₂, vector chiral, TLL2, dimer, and ferromagnetic phases. We briefly summarize the characteristics of each phase. In the following sections, we discuss in detail our numerical results for correlation functions and effective theories for each phase. In Sec. III, we consider the TLL1 phase, which appears in small J_2/J_1 regime. The correlation functions obtained with the DMRG method are shown to be fitted well to analytic forms obtained from a bosonization theory for a weakly-perturbed single Heisenberg spin chain, and the decay exponents of the spin correlation functions are estimated accurately. This analysis reveals that the dominant correlation function changes from the staggered transverse-spin correlation to incommensurate longitudinal-spin one as J_2/J_1 increases. In Sec. IV, we discuss the SDW₂ phase, which appears at larger J_2/J_1 . From the fitting of numerical data to bosonization theory, we show that the low-energy excitations are described by a one-component TLL with quasi-long-ranged dominant incommensurate longitudinal-spin and subleading nematic correlations and short-ranged transverse-spin correlation. Section V discusses the 1/3-plateau phase. We show that the numerically found up-up-down spin structure is understood in terms of the bosonization theories for the neighboring TLL1 and SDW₂ phases. In Sec. VI, we consider the vector chiral phase, which is also a one-component TLL. The fitting analysis shows that the vector chiral phase is characterized by the vector chiral LRO and the incommensurate quasi-LRO of the transverse spins. In Sec. VII, we develop a two-component TLL theory, i.e., two free boson theories (central charge $c = 1 + 1$), as a low-energy effective theory for the TLL2 phase. We confirm the central charge $c = 2$ through numerical computation of entanglement entropy. The

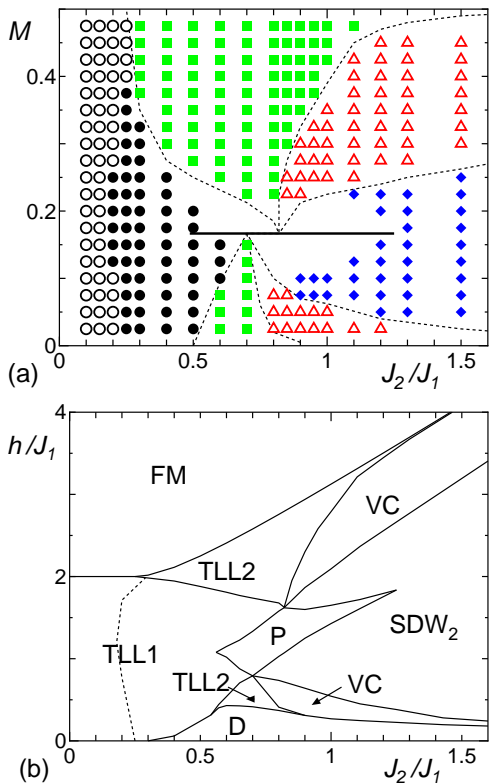


FIG. 1: (Color online) Magnetic phase diagram of the spin-1/2 antiferromagnetic zigzag ladder (a) in the J_2/J_1 versus M plane and (b) in the J_2/J_1 versus h/J_1 plane. In (a), symbols represent parameter points for which their ground-state phases are identified: Open (○) and solid (●) circles represent the TLL1 phase with dominant transverse- and longitudinal-spin correlation, respectively. Diamonds (◇), triangles (△), and squares (□) respectively represent the SDW₂, vector chiral, and TLL2 phases. The solid line shows the 1/3-plateau phase. The dotted curves are the guide for the eye. In (b), symbols “P”, “VC”, “D”, and “FM” indicate the 1/3 plateau, vector chiral, dimer, and ferromagnetic (fully polarized) phases, respectively. The phase boundaries shown by solid lines are obtained in Ref. 21 from the numerical results of magnetization curves, except for the boundaries between the vector chiral and TLL2 phases which are obtained from the analysis of correlation functions in the present paper. The dotted line in the TLL1 phase represents the crossover line between the transverse- and longitudinal-spin dominant regimes.

consistency between the effective theory and the DMRG result is shown by examining a few dominant Fourier components in the local magnetization profile near open boundaries. Section VIII contains summary and discussions on implications of our results to real quasi-1D compounds with weak interchain couplings.

II. PHASE DIAGRAM

Figure 1 presents the magnetic phase diagram based on the numerical results obtained in this paper as well as in previous studies. The diagram is shown in the J_2/J_1 versus magnetization M plane in Fig. 1(a) and in the J_2/J_1 versus h/J_1 plane in Fig. 1(b), where $M = (1/L) \sum_l s_l^z$ is the magnetization per site and L the system size. The system exhibits at least four critical phases, i.e., TLL1, TLL2, vector chiral, and SDW₂ phases, in addition to three gapped phases including the dimer phase at $M = 0$, the 1/3-plateau phase ($M = 1/6$), and the ferromagnetic phase ($M = 1/2$).

It has been revealed that the magnetization process of the zigzag ladder (1) has remarkable features.^{21,35–37} For small J_2/J_1 ($0.25 \leq J_2/J_1 \lesssim 0.7$), the magnetization curve has at most two cusp singularities at higher and lower fields, $h = h_{c1}$ and h_{c2} , which correspond to boundaries between the TLL1 and TLL2 phases. A magnetization plateau also appears at $M = 1/6$ for $0.487 < J_2/J_1 \lesssim 1.25$ and $h_{p1} < h < h_{p2}$.^{21,37} For large J_2/J_1 , the magnetization process exhibits two-spin flips with $\Delta S_{\text{tot}}^z = 2$ in an intermediate field region $h_{m1} < h < h_{m2}$. See Figs. 2 and 3 in Ref. 21 for these results. At zero magnetization, the ground state is gapless for $J_2/J_1 < 0.2411$ and dimerized for $0.2411 < J_2/J_1$. The spin gap in the dimerized phase vanishes at a critical field h_d . The ground state is fully polarized above the saturation field h_s . The critical fields h_{c1} , h_{c2} , h_{p1} , h_{p2} , h_{m1} , h_{m2} , h_d , and h_s are plotted in Fig. 1(b) with solid lines.

To reveal the nature of ground states in each region, we have calculated several correlation functions, using the DMRG method, for the system with up to $L = 160$ spins with open boundaries. We have kept typically 300 block states in the calculation (up to 400 states for some cases), and confirmed the convergence of the calculation by checking the dependence of results on the number of kept states. We have calculated the longitudinal-spin correlation function $\langle s_l^z s_{l'}^z \rangle$, the transverse-spin correlation function $\langle s_l^x s_{l'}^x \rangle$, the vector chiral correlation function $\langle \kappa_l^{(n)} \kappa_{l'}^{(n')} \rangle$ with $n, n' = 1, 2$, the nematic (two-magnon) correlation function $\langle s_l^+ s_{l+1}^+ s_{l'}^- s_{l'+1}^- \rangle$, and the local spin polarization $\langle s_l^z \rangle$, where $\langle \dots \rangle$ denotes the expectation value in the ground state. To lessen the open-boundary effects, we have computed the two-point correlation functions for several pairs of (l, l') with fixed distance $r = |l - l'|$ and taken their average for the estimate of the correlation at the distance r . In the following, we use the notation $\langle \dots \rangle_{\text{av}}$ for the averaged correlation functions.

Figure 2 shows typical spatial dependence of averaged correlation functions in the critical phases. We note that the bending-down behaviors of the averaged correlation functions seen for large distance (e.g., $r \gtrsim 100$ for $L = 160$) are due to boundary effects and should not be confused with intrinsic behaviors in the bulk. Ana-

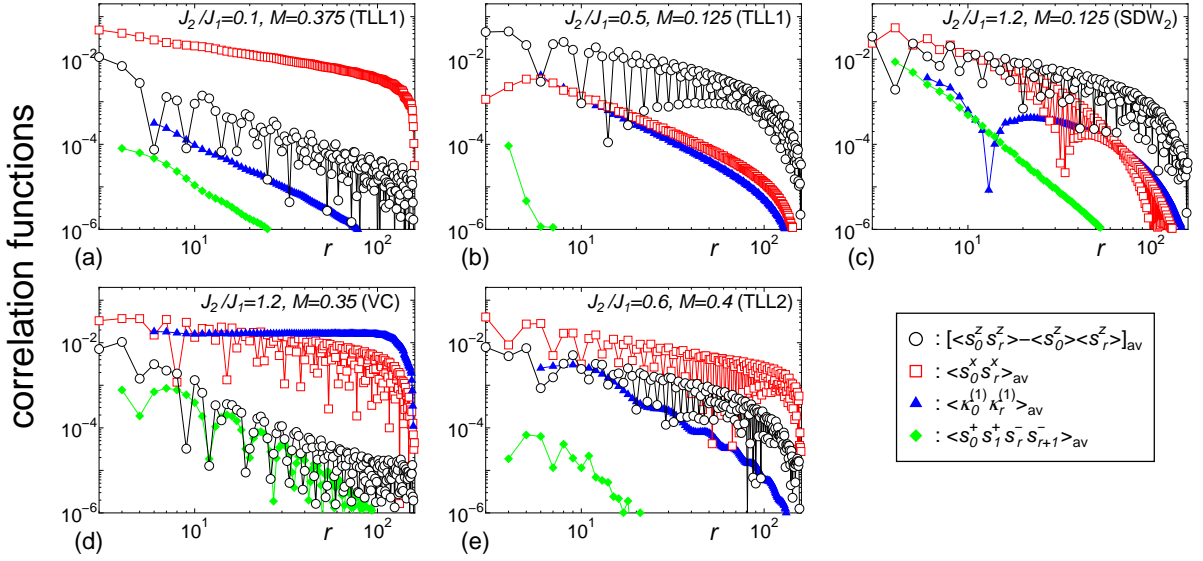


FIG. 2: (Color online) Typical spatial dependence of correlation functions in critical phases; (a) TLL1 phase (transverse-spin correlation dominant), (b) TLL1 phase (longitudinal-spin correlation dominant), (c) SDW₂ phase, (d) vector chiral phase, and (e) TLL2 phase. Absolute values of the averaged correlation functions are plotted.

lyzing the long-distance behavior of correlation functions in each parameter regime, we have determined the low-energy effective theory for each phase. The parameter points in the phase diagram at which numerical results are explained successfully by the effective low-energy theory of the corresponding phase are shown with symbols in Fig. 1(a). We summarize properties of each phase below.

TLL1 phase: In small J_2/J_1 regime, the ground state is adiabatically connected to the one-component TLL of the antiferromagnetic Heisenberg chain with only J_1 under magnetic field. For relatively large J_2/J_1 ($0.25 \leq J_2/J_1$) the boundaries of the TLL1 phase are defined by the cusp singularities in the magnetization curve.^{21,35} In this phase, both the longitudinal-spin fluctuation $\langle s_0^z s_r^z \rangle - \langle s_0^z \rangle \langle s_r^z \rangle$ and transverse-spin correlation functions $\langle s_0^x s_r^x \rangle$ decay algebraically. The former shows incommensurate oscillations with a wavenumber $Q = \pi(1 \pm 2M)$, while the latter is staggered, $Q = \pi$. The numerical estimation of the decay exponents, shown in Sec. III, indicates that the dominant correlation function changes from the staggered transverse-spin correlation to incommensurate longitudinal-spin correlation as J_2/J_1 increases [see Figs. 2 (a) and (b)]. The TLL1 phase is thus divided by the crossover line into two regions of different dominant correlations, as shown in Fig. 1.

SDW₂ phase: For large J_2/J_1 , there is a phase where the magnetization process changes by the steps of $\Delta S_{\text{tot}}^z = 2$.²¹ We show in Sec. IV that this phase is described by a one-component TLL theory, which was originally derived from the weakly-coupled AF Heisenberg chains in the limit $J_2/J_1 \gg 1$.^{22,41,50,52} The phase is characterized by the quasi-long-ranged longitudinal-spin and nematic correlation functions, $\langle s_0^z s_r^z \rangle - \langle s_0^z \rangle \langle s_r^z \rangle$

and $\langle s_0^+ s_1^+ s_r^- s_{r+1}^- \rangle$, which are dual to each other, and by the short-ranged transverse-spin correlation function $\langle s_0^x s_r^x \rangle$ reflecting a finite energy gap to single-spin-flip excitations, as shown in Fig. 2(c). The longitudinal-spin correlation is incommensurate with the wavenumber $Q_2 = \pm\pi(1/2 + M)$. Numerical analyses of correlation functions reveal that the longitudinal-spin correlation function is dominant in the whole parameter region of this phase. We thus call this phase the SDW₂ phase. We note that the same phase has been found in the zigzag ladder (1) with ferromagnetic J_1 and AF J_2 as well.^{22,23,48–53}

1/3-plateau phase: At one third of the saturated magnetization, $M = 1/6$, there is a magnetization-plateau phase in the intermediate parameter region $0.487 \lesssim J_2/J_1 \lesssim 1.25$.^{21,37} This phase is characterized by a field-induced excitation gap and a spontaneous breaking of translational symmetry accompanied by a magnetic LRO of the up-up-down structure. The ground state is three-fold degenerate. As shown in Sec. V, all two-point correlation functions exhibit exponential decay, in accordance with the fully-gapped nature of the phase.

Vector Chiral phase: The vector chiral phase is characterized by the LRO of the vector chirality $\kappa^{(n)}$ as well as quasi-LRO of incommensurate transverse spins, which decays algebraically in space. The discrete Z_2 symmetry corresponding to the parity about a bond center is broken spontaneously and the ground state is doubly degenerate in the thermodynamic limit. This vector chiral state is a quantum counterpart of the classical helical state. Though the classical helical state appears in $1/4 < J_2/J_1$ for arbitrary magnetization, the quantum vector chiral phase is found only in two narrow regions

separated by the SDW₂ and 1/3-plateau phases,^{42,43} see Fig. 1. We show that the vector chiral phase is also described by a one-component TLL theory which can be formulated starting from the two weakly-coupled AF Heisenberg chains for $J_2/J_1 \gg 1$.^{32,41} The correlation functions in this phase will be discussed in Sec. VI.

TLL2 phase: The TLL2 phase occupies two parameter regions adjacent to the TLL1 phase and the vector chiral phase. The TLL2 phase is described as two Gaussian conformal field theories (central charge $c = 1 + 1$), or a two-component TLL, having two flavors of free massless bosonic fields as its low-energy excitations. In the Jordan-Wigner fermion representation, fermions have two separate Fermi seas, and the two bosonic fields represent particle-hole excitations near the two sets of Fermi points. In the TLL2 phase all correlation functions decay algebraically and have incommensurate wave numbers which are linear functions of the two Fermi momenta of Jordan-Wigner fermions. We will discuss these properties and the low-energy effective theory in Sec. VII.

Dimer phase: For $J_2/J_1 > 0.2411$ and at $M = 0$, the ground state of the J_1 - J_2 AF Heisenberg spin chain is spontaneously dimerized.^{25–31} The ground state is doubly degenerate in the thermodynamic limit, and there is a gap to lowest excitation.

Ferromagnetic phase: When applied magnetic field is larger than the saturation field, $h > h_s$, the ground state is in the ferromagnetic phase with saturated magnetization $M = 1/2$. As the field decreases, the fully-polarized ground state is destabilized by softening of single-magnon excitations, which have the dispersion,

$$\varepsilon_k = J_1(\cos k - 1) + J_2(\cos 2k - 1) + h. \quad (6)$$

When $J_2/J_1 < 1/4$, the magnon dispersion has a single minimum at $k = \pi$, while, when $J_2/J_1 > 1/4$, there are two energy minima at $k = \pm \arccos(-J_1/4J_2)$. The saturation field h_s is given by $h_s/J_1 = 2$ for $J_2/J_1 < 1/4$ and $h_s/J_1 = 2J_2/J_1 + 1 + J_1/(8J_2)$ for $J_2/J_1 > 1/4$.

III. TLL1 PHASE

In this section, we discuss the TLL1 phase appearing for small J_2/J_1 . Since the parameter space of this phase includes the AF Heisenberg chain with $J_2 = 0$, we naturally expect that the TLL1 phase should share the same properties with the single Heisenberg chain. Here, we first briefly review the TLL theory for the AF Heisenberg chain with weak J_2 coupling. We then compare the theory with the numerical results of correlation functions for the zigzag chain (1) with $J_2 > 0$.

It is well known that the low-energy properties of a single Heisenberg chain under magnetic field ($|M| < \frac{1}{2}$ and $J_2 = 0$) is described as a TLL.⁴⁶ Since the (leading) operator generated from weak J_2 coupling is irrelevant in applied magnetic field (and marginally irrelevant without magnetic field) in the renormalization-group sense,

the low-energy effective theory for small J_2/J_1 is adiabatically connected to the TLL theory of the single AF Heisenberg chain ($J_2 = 0$). Hence the low-energy excitations in the TLL1 phase are free massless bosons governed by the Gaussian model,

$$\tilde{\mathcal{H}}_0 = \frac{v}{2} \int dx \left[K \left(\frac{d\theta}{dx} \right)^2 + \frac{1}{K} \left(\frac{d\phi}{dx} \right)^2 \right], \quad (7)$$

where (ϕ, θ) are bosonic fields satisfying the equal-time commutation relation $[\phi(x), \partial_y \theta(y)] = i\delta(x - y)$. The TLL parameter K is a function of J_2/J_1 and M . We have taken the lattice spacing to be one and identify the continuous coordinate x with the site index l . The spin velocity v is of order J_1 , except for the saturation limit $M \rightarrow 1/2$, where $v \rightarrow 0$. The spin operators s_l can be expressed in terms of the bosonic fields as

$$s_l^z = M + \frac{1}{\sqrt{\pi}} \frac{d\phi(x)}{dx} - (-1)^l a \sin[2\pi M l + \sqrt{4\pi}\phi(x)] + \dots, \quad (8)$$

$$s_l^\pm = (-1)^l b e^{i\sqrt{\pi}\theta(x)} + b' e^{i\sqrt{\pi}\theta(x)} \sin[2\pi M l + \sqrt{4\pi}\phi(x)] + \dots, \quad (9)$$

where a , b , and b' are nonuniversal positive constants, whose numerical values are known at $J_2 = 0$.^{54–56} Equations (7), (8), and (9) define the effective theory for the TLL1 phase, with which asymptotic forms of spin correlation functions are obtained as

$$\langle s_0^z s_r^z \rangle = M^2 - \frac{\eta}{4\pi^2 r^2} + A_1^z \frac{(-1)^r \cos(2\pi M r)}{|r|^\eta} + \dots \quad (10)$$

$$\langle s_0^x s_r^x \rangle = A_0^x \frac{(-1)^r}{|r|^{1/\eta}} - A_1^x \frac{\cos(2\pi M r)}{|r|^{\eta+1/\eta}} + \dots, \quad (11)$$

where $A_1^z = a^2/2$, $A_0^x = b^2/2$, $A_1^x = b'^2/4$ (with appropriate short-distance regularization), and the decay exponent η is related to the TLL parameter K by $\eta = 2K$. Equations (10) and (11) tell us that for $\eta > 1$ the staggered transverse-spin correlation function $\langle s_l^x s_{l'}^x \rangle$ is dominant, while the incommensurate longitudinal-spin correlation $\langle s_l^z s_{l'}^z \rangle$ with a wavenumber $Q = \pi(1 \pm 2M)$ is dominant for $\eta < 1$. At $J_2 = 0$ the decay exponent η can be calculated exactly using Bethe ansatz;^{59,60} η increases monotonically as M increases, from $\eta = 1$ at $M = 0$ to $\eta = 2$ for $M \rightarrow 1/2$. Therefore, at $J_2 = 0$, the transverse-spin correlation $\langle s_0^x s_r^x \rangle$ is always the most-slowly decaying one for $0 < M < 1/2$. For finite $J_2 > 0$, the exact value of the exponent η is known in the limit $M \rightarrow 0$. For $J_2/J_1 < 0.2411$ where the ground state at $M = 0$ is in the TLL1 phase, $\eta = 1$ at $M = 0$ because of the SU(2) symmetry. On the other hand, for $J_2/J_1 > 0.2411$, i.e., when the ground state at $M = 0$ is in the dimer phase,^{57,58} $\eta \rightarrow 1/2$ as $M \rightarrow 0$. This means that η is singular at $J_2/J_1 = (J_2/J_1)_c$ and $M = 0$.

One can also derive the (same) effective theory for the TLL1 phase, starting from the saturation limit for

$0 < J_2/J_1 < 1/4$. In this limit the system can be viewed as a dilute gas of interacting hard-core bosons (magnons) with one flavor, as the magnon dispersion (6) has a single minimum at $k = \pi$. The hydrodynamic theory for the one-flavor interacting bosons is nothing but the TLL theory, Eq. (7).⁴⁶ This approach naturally gives the same asymptotic forms of spin correlators as Eqs. (8) and (9). Furthermore, in the saturation limit $M \rightarrow 1/2$, $\eta \rightarrow 2$ in the TLL1 phase (i.e., $J_2/J_1 < 1/4$), since the dilute limit of the hard-core bose gas is equivalent to a free fermion gas.

Next we discuss our DMRG results of the transverse and longitudinal spin correlation functions $\langle s_l^x s_{l'}^x \rangle$ and $\langle s_l^z s_{l'}^z \rangle$ and the local spin polarization $\langle s_l^z \rangle$. To achieve better numerical convergence and efficiency, the DMRG calculation was done for finite systems (L spins) with open boundaries. We thus compare the numerical results with the correlation functions calculated analytically from the effective theory (7) by imposing appropriate boundary conditions on the bosonic field ϕ .⁵⁴⁻⁵⁶ To this end, we have taken the Dirichlet boundary conditions $\phi(\delta) = \phi(L+1-\delta) = 0$,⁶¹ where δ is a free parameter to be determined later. For example, spatial dependence of the magnetization is given by

$$\langle s_l^z \rangle = z(l; q) \equiv \frac{q}{2\pi} - a \frac{(-1)^l \sin[q(l-\delta)]}{f_{\eta/2}(2(l-\delta))}, \quad (12)$$

where

$$q = \frac{2\pi LM}{L+1-2\delta}, \quad (13)$$

and

$$f_\alpha(x) = \left[\frac{2(L+1-2\delta)}{\pi} \sin\left(\frac{\pi|x|}{2(L+1-2\delta)}\right) \right]^\alpha. \quad (14)$$

In the limit $l \ll L$, Eq. (12) reduces to

$$\langle s_l^z \rangle = M - \frac{(-1)^l a}{[2(l-\delta)]^{\eta/2}} \sin[2\pi M(l-\delta)]. \quad (15)$$

The presence of open boundaries gives rise to “Friedel oscillations” in the local magnetization. The wave number of the oscillations is “ $2k_F$ ” of the Jordan-Wigner fermions, which equals $Q = \pi(1 \pm 2M)$ for $L \gg 1$. Similarly, the longitudinal and transverse spin correlation functions are modified by boundary contributions as

$$\begin{aligned} \langle s_l^z s_{l'}^z \rangle &= Z(l, l'; q) \\ &\equiv \left(\frac{q}{2\pi} \right)^2 - \frac{\eta}{4\pi^2} \left[\frac{1}{f_2(l-l')} + \frac{1}{f_2(l+l'-2\delta)} \right] - \frac{qa}{2\pi} \left[\frac{(-1)^l \sin[q(l-\delta)]}{f_{\eta/2}(2(l-\delta))} + \frac{(-1)^{l'} \sin[q(l'-\delta)]}{f_{\eta/2}(2(l'-\delta))} \right] \\ &\quad + \frac{(-1)^{l-l'} a^2}{2f_{\eta/2}(2(l-\delta))f_{\eta/2}(2(l'-\delta))} \left\{ \cos[q(l-l')] \frac{f_\eta(l+l'-2\delta)}{f_\eta(l-l')} - \cos[q(l+l'-2\delta)] \frac{f_\eta(l-l')}{f_\eta(l+l'-2\delta)} \right\} \\ &\quad - \frac{\eta a}{2\pi} \left\{ \frac{(-1)^l \cos[q(l-\delta)]}{f_{\eta/2}(2(l-\delta))} [g(l+l'-2\delta) + g(l-l')] + \frac{(-1)^{l'} \cos[q(l'-\delta)]}{f_{\eta/2}(2(l'-\delta))} [g(l+l'-2\delta) - g(l-l')] \right\}, \quad (16) \end{aligned}$$

$$\langle s_l^z s_{l'}^z \rangle - \langle s_l^z \rangle \langle s_{l'}^z \rangle = Z(l, l'; q) - z(l; q)z(l'; q), \quad (17)$$

$$\begin{aligned} \langle s_l^x s_{l'}^x \rangle &= X(l, l'; q) \\ &\equiv \frac{f_{1/2\eta}(2(l-\delta))f_{1/2\eta}(2(l'-\delta))}{f_{1/\eta}(l-l')f_{1/\eta}(l+l'-2\delta)} \left\{ \frac{(-1)^{l-l'} b^2}{2} + \frac{\text{sgn}(l-l')bb'}{2} \left[\frac{(-1)^{l'} \cos[q(l-\delta)]}{f_{\eta/2}(2(l-\delta))} - \frac{(-1)^l \cos[q(l'-\delta)]}{f_{\eta/2}(2(l'-\delta))} \right] \right. \\ &\quad \left. - \frac{b'^2}{4f_{\eta/2}(2(l-\delta))f_{\eta/2}(2(l'-\delta))} \left[\cos[q(l+l'-2\delta)] \frac{f_\eta(l-l')}{f_\eta(l+l'-2\delta)} + \cos[q(l-l')] \frac{f_\eta(l+l'-2\delta)}{f_\eta(l-l')} \right] \right\}, \quad (18) \end{aligned}$$

where

$$g(x) = \frac{\pi}{2(L+1-2\delta)} \cot\left[\frac{\pi x}{2(L+1-2\delta)}\right]. \quad (19)$$

In the limit $|L/2 - l| \ll L$ and $|L/2 - l'| \ll L$, boundary effects go away, and Eqs. (16) and (18) reduce to Eqs. (10) and (11). In the fitting procedure discussed below,

we have optimized δ to achieve the best fitting of $\langle s_l^z \rangle$ and $\langle s_l^z s_{l'}^z \rangle - \langle s_l^z \rangle \langle s_{l'}^z \rangle$, whereas we set $\delta = 0$ for $\langle s_l^x s_{l'}^x \rangle$ as it has turned out that the numerical data of $\langle s_l^x s_{l'}^x \rangle$ can be fitted sufficiently well without optimizing δ .

Figure 3 shows DMRG data of $\langle s_l^z \rangle$, $\langle s_l^z s_{l'}^z \rangle - \langle s_l^z \rangle \langle s_{l'}^z \rangle$, and $\langle s_l^x s_{l'}^x \rangle$ for $(J_2/J_1, M) = (0.1, 0.375)$ and $(0.5, 0.125)$. In the same figures, we show the fits to Eqs. (12), (17),

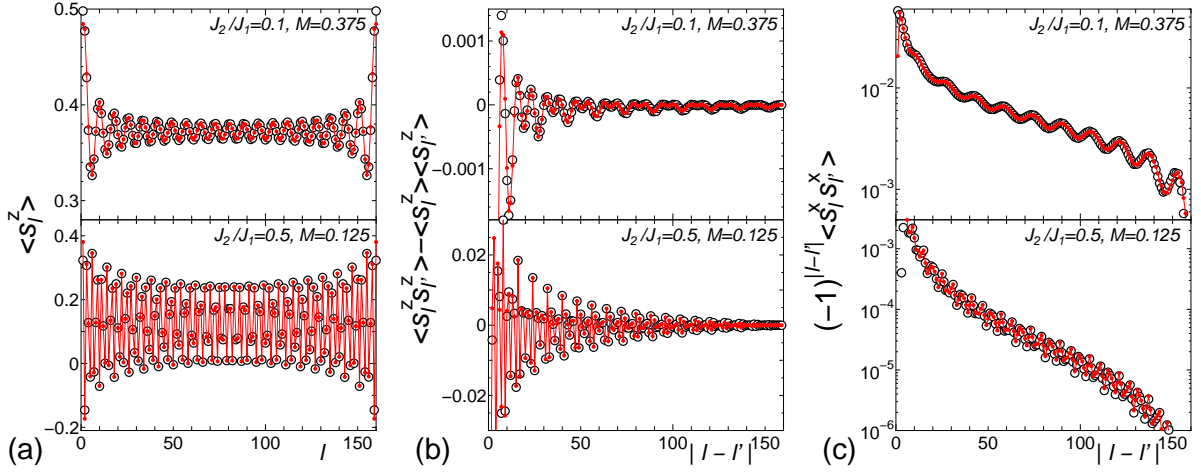


FIG. 3: (Color online) Correlation functions in the antiferromagnetic zigzag ladder with $L = 160$ spins in the TLL1 phase; (a) local spin polarization $\langle s_l^z \rangle$, (b) longitudinal-spin fluctuation $\langle s_l^z s_{l'}^z \rangle - \langle s_l^z \rangle \langle s_{l'}^z \rangle$, and (c) transverse-spin correlation function $\langle s_l^x s_{l'}^x \rangle$. The upper and lower panels show the results for $(J_2/J_1, M) = (0.1, 0.375)$ and $(0.5, 0.125)$, respectively. The open symbols represent the DMRG data and the solid lines and circles are fits to Eqs. (12), (17), and (18). In (b) and (c), the data for $l = L/2 - [r/2]$ and $l' = L/2 + [(r+1)/2]$ are shown as a function of $r = |l - l'|$.

and (18). Clearly, the fits are in excellent agreement with the numerical results. We emphasize that only three fitting parameters, η , δ , and a (η , b , and b') are used in the fitting of $\langle s_l^z \rangle$ and $\langle s_l^z s_{l'}^z \rangle - \langle s_l^z \rangle \langle s_{l'}^z \rangle$ ($\langle s_l^x s_{l'}^x \rangle$). We have obtained almost the same good quality of fits for the parameter points marked by open and solid circles in Fig. 1(b), which cover almost the entire region of the TLL1 phase. These results thus demonstrate that the TLL1 phase is described by the effective TLL theory given by Eqs. (7), (8), and (9), which is indeed the same TLL theory as that of the AF Heisenberg chain ($J_2 = 0$).

Figure 4 shows dependence of the exponent η on the magnetization M in the TLL1 phase, obtained from the fitting of the transverse-spin correlation $\langle s_l^x s_{l'}^x \rangle$. Similar estimates of η are obtained from the other correlators (not shown). For small J_2/J_1 , η exhibits essentially the same behavior as a function of M as $\eta(M)$ at $J_2 = 0$; for $J_2/J_1 \lesssim 0.15$, η increases monotonically from the universal value $\eta = 1$ at $M = 0$ to $\eta = 2$ at $M \rightarrow 1/2$ as M increases. In this regime the transverse-spin correlation $\langle s_0^x s_l^x \rangle$ is dominant for any M . The situation changes as J_2/J_1 gets larger. With increasing J_2/J_1 , η decreases and becomes smaller than 1 at $J_2/J_1 = 0.2$ for intermediate magnetization M . As J_2/J_1 is further increased in the TLL1 phase, the exponent η gets smaller than 1 for any M . Thus, the system undergoes a crossover from the small J_2/J_1 region with the dominant staggered transverse-spin correlation to the large J_2/J_1 region where the incommensurate longitudinal-spin correlation with $Q = \pi(1 \pm 2M)$ is dominant. The crossover line is shown in the phase diagram, Fig. 1. The result is consistent with the earlier study,⁶² in which η was estimated at $M = 1/6, 1/4$ and $1/3$ for small systems. Such a crossover between ground states with the different dom-

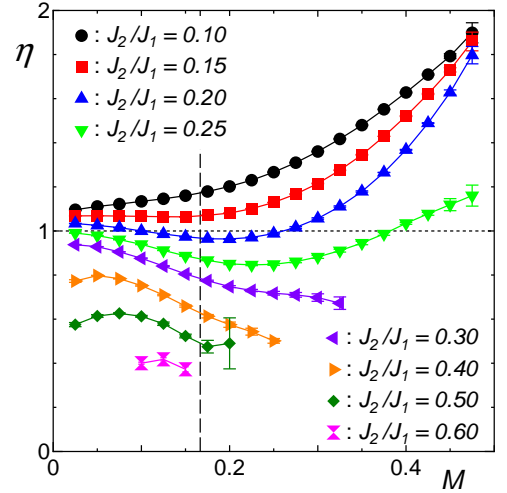


FIG. 4: (Color online) M dependence of the exponent η for the TLL1 phase estimated from the fitting of $\langle s_l^x s_{l'}^x \rangle$ for the antiferromagnetic zigzag ladder with $L = 160$ spins. The error bars represent the difference of the estimates obtained from the fitting of the data of different ranges. The vertical dashed line corresponds to $M = 1/6$ where the $1/3$ -plateau can appear for large J_2/J_1 . The dotted line at $\eta = 1$ is the guide for the eye. The exponent η relates to the parameter K as $\eta = 2K$ in the TLL theory for the TLL1 phase.

inant spin correlations has also been found for the J_1 - J_2 chain with bond alternation.^{63–66}

As mentioned above, η is expected to approach $1/2$ as $M \rightarrow 0$ for $J_2/J_1 > (J_2/J_1)_c = 0.2411$. Our numerical results at $J_2/J_1 = 0.5$ are consistent with this theoretical prediction. However, as J_2/J_1 approaches $(J_2/J_1)_c$ from

above, the value of η at the smallest $M = 0.025$ becomes larger towards $\eta = 1$, the value expected for $J_2/J_1 < (J_2/J_1)_c$. This implies that η increases very rapidly from $1/2$ at small M for this parameter regime of $J_2/J_1 \lesssim 0.3$, where the spin gap in the dimer ground state at $M = 0$ is exponentially small (thereby small M is sufficient to wipe out dimer instability).

The data points for $0.3 \leq J_2/J_1 \leq 0.5$ end at the boundary to the TLL2 phase for larger M . Our results seem to indicate that η changes continuously along the TLL1-TLL2 phase boundary.

When the magnetization is close to $M = 1/6$, the TLL1 phase has an instability to the $1/3$ -plateau phase. In the Jordan-Wigner fermion picture, the instability is caused by umklapp scattering of three fermions, and the $1/3$ -plateau phase corresponds to a density wave state of the fermions.^{67,68} The three-particle umklapp scattering is irrelevant at small J_2/J_1 but becomes relevant for larger J_2/J_1 . This explains why the $1/3$ -plateau phase emerges at $J_2/J_1 \gtrsim 0.5$ in the phase diagram (Fig. 1), as we discuss below.

The effective Hamiltonian yielding the $1/3$ -plateau has the form⁶⁷⁻⁶⁹

$$\tilde{H} = \tilde{H}_0 + \lambda \int dx \sin[\pi(6M - 1)x + 3\sqrt{4\pi}\phi(x)], \quad (20)$$

where \tilde{H}_0 is the Gaussian model (7) for the TLL1 phase and λ is the coupling constant for the three-particle umklapp scattering. The umklapp term is accompanied by an oscillating factor with a wavenumber $\pi(6M - 1) \equiv 3\pi(1 + 2M)$ and becomes uniform at $M = 1/6$. If we fix the magnetization at $M = 1/6$ and increase J_2/J_1 , then the three-particle umklapp term becomes relevant for $K < 2/9$ ($\eta < 4/9$). Indeed, we see in Fig. 4 that the estimates of η near $M = 1/6$ are larger than $4/9$ for $J_2/J_1 \leq 0.4$ and become close to $4/9$ at $J_2/J_1 = 0.5$. This result is consistent with the estimated critical value $(J_2/J_1)_{p1} = 0.487$ which was obtained from the analysis of the level spectroscopy in Ref. 37. For $J_2/J_1 > (J_2/J_1)_{p1}$ we can approach the $1/3$ -plateau phases by changing the magnetic field h . This is in the universality class of commensurate-incommensurate transition.^{57,79} In this case we expect that, as $M \rightarrow 1/6$, the TLL parameter K approaches $1/9$, or, equivalently, $\eta \rightarrow 2/9$.⁵⁷ On the other hand, our numerical data for $J_2/J_1 = 0.6$ seem to be much larger than the theoretical value $2/9$ at $M \rightarrow 1/6$. Although this disagreement might suggest that there exist rather large errors in the estimates of η for large J_2/J_1 , we rather expect that η for $J_2/J_1 = 0.6$ should actually show rapid decrease very close to $M = 1/6$ to recover the predicted behavior, $\eta \rightarrow 2/9$ as $M \rightarrow 1/6$. Numerical verification of this would require calculations on much larger systems.

IV. SDW₂ PHASE

In this section we discuss the SDW₂ phase. This phase is characterized by two-spin flips $\Delta S^z = 2$ in the magnetization process.^{21,70} The parameter space of the SDW₂ phase extends to large J_2/J_1 , see Fig. 1. Its low-energy effective field theory is obtained in the limit $J_2/J_1 \rightarrow 1$, and we will give a short review on it below.^{22,41,50,52} Then, by comparing our DMRG data of correlation functions for $J_1/J_2 \gtrsim 1$ with the analytic results, we demonstrate that the effective theory is valid in the whole parameter space of the SDW₂ phase, as expected from the principle of adiabatic continuity.⁸⁰

In the limit $J_2 \gg J_1$, the zigzag spin ladder (1) can be viewed as two Heisenberg chains with *nearest-neighbor* exchange J_2 coupled by weak interchain exchange J_1 . It is natural to bosonize each chain separately first and then incorporate the interchain coupling J_1 perturbatively. In this scheme, the original spin operators are written as

$$\begin{aligned} s_{2j+n}^z &= M + \frac{1}{\sqrt{\pi}} \frac{d\phi_n(\bar{x}_n)}{d\bar{x}} \\ &\quad - (-1)^j a \sin[2\pi M j + \sqrt{4\pi}\phi_n(\bar{x}_n)] + \cdots, \quad (21) \\ s_{2j+n}^+ &= (-1)^j b e^{i\sqrt{\pi}\theta_n(\bar{x}_n)} \\ &\quad + b' e^{i\sqrt{\pi}\theta_n(\bar{x}_n)} \sin[2\pi M j + \sqrt{4\pi}\phi_n(\bar{x}_n)] + \cdots, \quad (22) \end{aligned}$$

where (ϕ_n, θ_n) are the bosonic fields for each chain $n = 1, 2$. The coordinate \bar{x} is related to the site index $l = 2j + n$ ($n = 1, 2$) as $\bar{x}_1 = j - 1/4$ and $\bar{x}_2 = j + 1/4$. The low-energy theory of each AF Heisenberg chain has the same form as \tilde{H}_0 in Eq. (7). The bosonized form of the interchain coupling J_1 can be found from Eqs. (21) and (22). We then obtain the effective Hamiltonian^{22,41,50,52}

$$\begin{aligned} \tilde{H} &= \sum_{\nu=\pm} \frac{v_\nu}{2} \int d\bar{x} \left[K_\nu \left(\frac{d\theta_\nu}{d\bar{x}} \right)^2 + \frac{1}{K_\nu} \left(\frac{d\phi_\nu}{d\bar{x}} \right)^2 \right] \\ &\quad + g_1 \int d\bar{x} \sin(\sqrt{8\pi}\phi_- + \pi M) \\ &\quad + g_2 \int d\bar{x} \frac{d\theta_+}{d\bar{x}} \sin(\sqrt{2\pi}\theta_-), \quad (23) \end{aligned}$$

where the interchain coupling gives the nonlinear interaction terms with the coupling constants

$$g_1 = J_1 a^2 \sin(\pi M), \quad g_2 = \frac{J_1}{2} \sqrt{2\pi} b^2 \quad (24)$$

in lowest order in J_1 . Here we have introduced symmetric (+) and antisymmetric (−) linear combinations of the bosonic fields, $\phi_\pm = (\phi_1 \pm \phi_2)/\sqrt{2}$, $\theta_\pm = (\theta_1 \pm \theta_2)/\sqrt{2}$. In lowest order in J_1 the TLL parameters K_\pm are given by

$$K_\pm = K \left(1 \mp \frac{J_1 K}{\pi v} \right), \quad (25)$$

where K is the TLL parameter of the decoupled Heisenberg chains.⁴¹ This suggests that K_+ is less than 1 and decreases with J_1 at the limit $J_1 \ll J_2$. The spin velocities v_{\pm} are of order J_2 in the weak-coupling regime, except for $M \rightarrow 1/2$ where $v_{\pm} \rightarrow 0$.

The effective Hamiltonian (23) has two competing interactions ($\propto g_1$ and g_2). The fate of the ground state is determined by which one of the two interactions grows faster in renormalization-group transformations. If the g_1 term is dominant, the SDW₂ phase is realized. We discuss this case below. On the other hand, if the g_2 term is most relevant, then the ground state is in the vector chiral phase; this case is discussed in Sec. VI.

Let us assume that the g_1 term wins the competition. Then the field ϕ_- is pinned at a minimum of the potential $g_1 \sin(\sqrt{8\pi}\phi_- + \pi M)$,

$$\langle \phi_- \rangle = -\sqrt{\frac{\pi}{8}} \left(\frac{1}{2} + M \right), \quad (26)$$

as $g_1 \propto J_1 > 0$. Since the pinned field ϕ_- can be taken as a constant, the difference of (the uniform part of) two neighboring spins vanishes, $s_{2j+1}^z - s_{2j+2}^z = \sqrt{2/\pi} \partial_{\bar{x}} \phi_- = 0$. This means that the two spins are bound and explains the steps $\Delta S_{\text{tot}}^z = 2$ in the magnetization process.⁵⁰ The dual field θ_- fluctuates strongly and we can therefore safely ignore the g_2 coupling. The antisymmetric sector (ϕ_-, θ_-) has an energy gap, which corresponds to the binding energy of the two-spin bound state.

Since the bosonic fields (ϕ_+, θ_+) in the symmetric sector are not directly affected by the relevant inter-chain couplings, they remain gapless and constitute the one-component TLL. The effective Hamiltonian for the SDW₂ phase is the Gaussian model,

$$\tilde{\mathcal{H}}_+ = \frac{v_+}{2} \int d\bar{x} \left[K_+ \left(\frac{d\theta_+}{d\bar{x}} \right)^2 + \frac{1}{K_+} \left(\frac{d\phi_+}{d\bar{x}} \right)^2 \right]. \quad (27)$$

Equations (21), (22), (26), and (27) represent the TLL theory for the SDW₂ phase.

Straightforward calculations yield the longitudinal-spin and nematic (two-magnon) correlation functions in the thermodynamic limit,

$$\langle s_0^z s_r^z \rangle = M^2 - \frac{\eta}{\pi^2 r^2} + \frac{\tilde{A}_1^z}{|r|^\eta} \cos \left[\pi r \left(\frac{1}{2} + M \right) \right] + \dots, \quad (28)$$

$$\begin{aligned} \langle s_0^+ s_1^+ s_r^- s_{r+1}^- \rangle &= \frac{(-1)^r \tilde{A}_0}{|r|^{1/\eta}} \\ &\quad - \frac{\tilde{A}_1(-1)^r}{|r|^{\eta+1/\eta}} \cos \left[\pi r \left(\frac{1}{2} + M \right) \right] + \dots, \end{aligned} \quad (29)$$

where the exponent $\eta = K_+$, and we have introduced positive numerical constants $\tilde{A}_{0,1}$ and \tilde{A}_1^z . These correlations are quasi-long-ranged and dual to each other. If $\eta < 1$, the incommensurate SDW correlation [the third

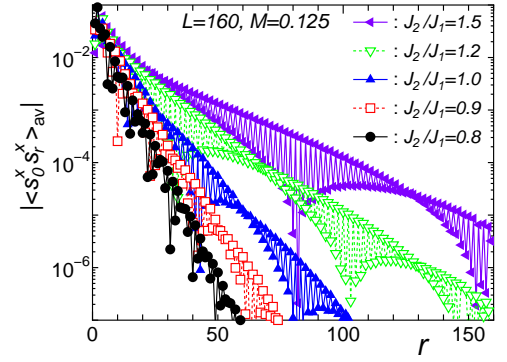


FIG. 5: (Color online) Absolute values of the averaged transverse-spin correlation function, $|\langle s_0^x s_r^x \rangle_{\text{av}}|$, in the antiferromagnetic zigzag ladder with $L = 160$ spins for $M = 0.125$ and several J_2/J_1 .

term in Eq. (28)] is the most dominant, while the staggered nematic correlation is the strongest for $\eta > 1$. The perturbative result (25) indicates that the incommensurate SDW correlation is dominant ($K_+ < 1$) for small J_1/J_2 . We will see below that this holds true for $J_1/J_2 \approx 1$ as well. The wavenumber of the SDW quasi-LRO is $Q_2 = \pm\pi(1/2 + M)$, which is distinct from that of incommensurate correlations in other phases and is characteristic of the SDW₂ phase. We note that in the SDW₂ phase of the *ferromagnetic* ($J_1 < 0$) J_1 - J_2 chain, the characteristic wavenumber is $Q = \pm\pi(1/2 - M)$.^{22,47} Such a spin-density-wave state with the incommensurate wave vector is also found in the spatially-anisotropic triangular antiferromagnet in magnetic field.⁹

The transverse-spin correlation function $\langle s_0^x s_r^x \rangle$ decays exponentially as the operator s_i^x includes the strongly disordered θ_- field. The exponential behavior is a direct consequence of the finite-energy cost for creating a single-magnon excitation and is a hallmark of the SDW₂ phase.

Let us discuss numerical results. Figure 2(c) shows typical behaviors of the averaged correlation functions in the SDW₂ phase. The longitudinal-spin and two-magnon correlation functions decay algebraically and the former is clearly dominant. By contrast, as shown in Fig. 5, the transverse-spin correlation decays exponentially. This can be seen as evidence for the appearance of two-magnon bound states in this parameter regime. The correlation length of transverse spins becomes larger with increasing J_2/J_1 . This is in accordance with the bosonization prediction that the energy gap for the single-spin excitation is generated by the cosine term with the coefficient $g_1 \sim J_1$ for $J_1/J_2 \ll 1$. We have found essentially the same behavior of the correlation functions as shown in Fig. 2(c) for the entire parameter region where the two-spin-flips with $\Delta S_{\text{tot}}^z = 2$ are observed in the magnetization process. After the dominant correlation function and the formation of two-magnon bound pairs, we call this phase the SDW₂ phase.

In order to estimate the exponent η and to further

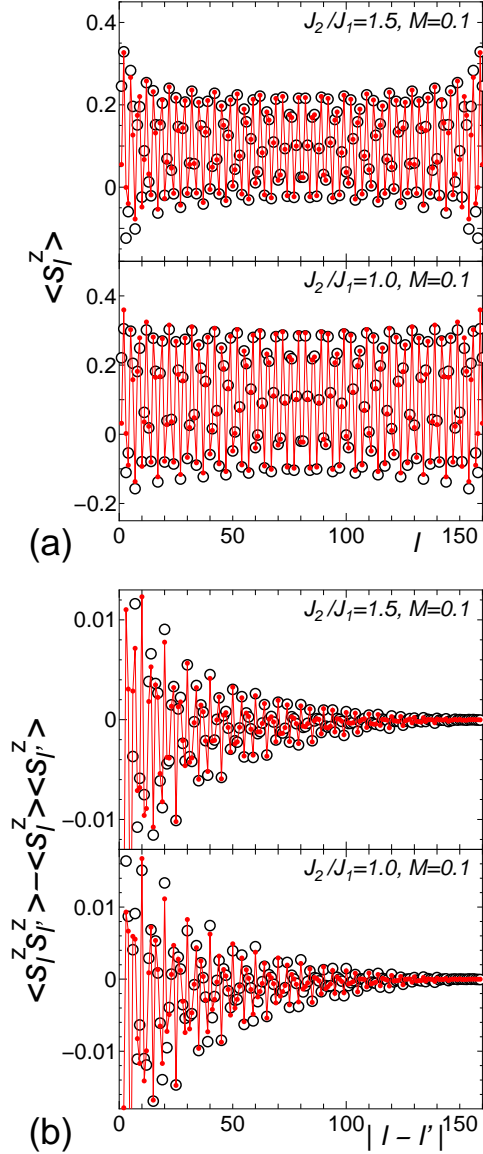


FIG. 6: (Color online) Correlation functions in the antiferromagnetic zigzag ladder with $L = 160$ spins in the SDW₂ phase; (a) local spin polarization $\langle s_l^z \rangle$ and (b) longitudinal-spin fluctuation $\langle s_l^z s_{l'}^z \rangle - \langle s_l^z \rangle \langle s_{l'}^z \rangle$. The upper and lower panels show the results for $(J_2/J_1, M) = (1.5, 0.1)$ and $(1.0, 0.1)$, respectively. The open symbols represent the DMRG data and the solid symbols are the result of fitting to Eqs. (30) and (31). In (b), the data for $l = L/2 - [r/2]$ and $l' = L/2 + [(r+1)/2]$ are shown as a function of $r = |l - l'|$.

demonstrate the validity of the effective theory for the SDW₂ phase, we fit the DMRG data of the local-spin polarization $\langle s_l^z \rangle$ and the longitudinal-spin fluctuation $\langle s_l^z s_{l'}^z \rangle - \langle s_l^z \rangle \langle s_{l'}^z \rangle$ to analytic forms obtained from the bosonization approach. Using Eqs. (21), (26), and (27) and applying the Dirichlet boundary condition in the same manner as in Sec. III, we obtain the correlators

for a finite open chain as

$$\langle s_l^z \rangle = \frac{1}{2} - 2z(l; \tilde{q}), \quad (30)$$

$$\langle s_l^z s_{l'}^z \rangle - \langle s_l^z \rangle \langle s_{l'}^z \rangle = 4[Z(l, l'; \tilde{q}) - z(l; \tilde{q})z(l'; \tilde{q})], \quad (31)$$

with

$$\tilde{q} = \frac{2\pi L}{L+1-2\delta} \left(\frac{1}{4} - \frac{M}{2} \right). \quad (32)$$

In the limit $l \ll L$, Eq. (30) reduces to

$$\langle s_l^z \rangle = M + \frac{2(-1)^l a}{[2(l-\delta)]^{\eta/2}} \sin \left[\left(\frac{\pi}{2} - \pi M \right) (l - \delta) \right], \quad (33)$$

showing Friedel oscillations with wavenumber $\pi(\frac{1}{2} + M)$.

Figure 6 shows DMRG results and their fits to Eqs. (30) and (31). The results for $J_2/J_1 = 1.5$ show that the numerical data at relatively large J_2/J_1 are fitted pretty well by the analytic forms. Note that only three fitting parameters, η , a , and δ , are used in the fitting procedure. For smaller J_2/J_1 , the fitting results become less satisfactory, presumably because a smaller value of η amplifies effects of both finite system size and higher-order terms omitted in the analytic forms (see also the discussion below for the estimate of η). Nevertheless the fitting still gives a rather good result at $J_2/J_1 = 1.0$ as well. This observation gives a strong support to the validity of the TLL theory for the SDW₂ phase. We emphasize that the successful fitting directly demonstrates that the characteristic wavenumber of the spin-density wave is $Q_2 = \pm\pi(1/2 + M)$, in accordance with the theory above. In the phase diagram in Fig. 1(a), we plot the parameter points where the fitting worked well, which cover almost the entire region of the SDW₂ phase. In the vicinity of the 1/3-plateau, however, good fitting results were not obtained due to the strong boundary effects.

In Fig. 7, we present the exponent η estimated from the fitting of the longitudinal-spin fluctuation $\langle s_l^z s_{l'}^z \rangle - \langle s_l^z \rangle \langle s_{l'}^z \rangle$. Although the estimates have rather large error bars coming from high sensitivity to the choice of the data range used in the fitting, we can safely conclude that the exponent for $J_2/J_1 \lesssim 1.5$ is always small, i.e., $\eta \lesssim 0.5$. This result reflects the fact that the longitudinal-spin correlation is the strongest in the SDW₂ phase. Furthermore, the data show the tendency that η increases with J_2/J_1 . Combining this observation with the perturbative result (25) for $J_2 \gg J_1$, we may expect that η increases monotonically with J_2/J_1 but less than 1 for the entire regime of $J_2/J_1 \gtrsim 1$. This means that the SDW₂ phase, with the dominant longitudinal-spin correlation, should extend from the intermediate coupling regime of $J_2/J_1 \sim 1$ to the limit $J_2/J_1 \rightarrow \infty$.

With decreasing J_2/J_1 , the SDW₂ phase appears to touch the 1/3-plateau phase. Here we discuss this plateau-nonplateau transition within the TLL theory for the SDW₂ phase. We can consider the effective Hamiltonian with a three-particle umklapp scattering,

$$\tilde{\mathcal{H}}'_+ = \tilde{\mathcal{H}}_+ + \tilde{\lambda} \int d\bar{x} \sin \left[\pi \bar{x} (6M - 1) + 3\sqrt{2}\pi \phi_+ \right], \quad (34)$$

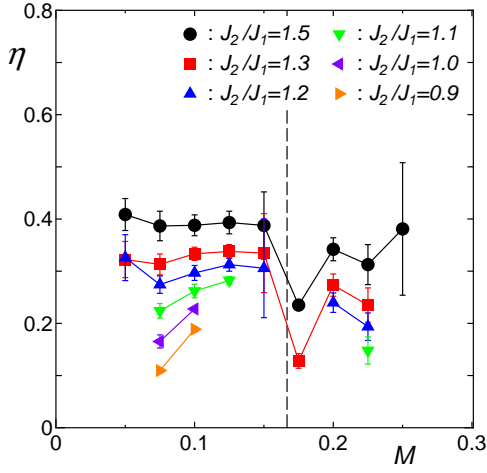


FIG. 7: (Color online) M dependence of the exponent η for the SDW_2 phase estimated from the fitting of $\langle s_l^z s_{l'}^z \rangle - \langle s_l^z \rangle \langle s_{l'}^z \rangle$ for the antiferromagnetic zigzag ladder with $L = 160$ spins. The error bars represent the difference of the estimates obtained from the fitting of the data of different ranges. The vertical dashed line corresponds to $M = 1/6$ where the $1/3$ -plateau can appear for small J_2/J_1 . The exponent η relates to the parameter K_+ as $\eta = K_+$ in the TLL theory for the SDW_2 phase.

where $\tilde{\mathcal{H}}_+$ is given in Eq. (27), and $\tilde{\lambda}$ is the coupling constant for three-particle umklapp scattering. The umklapp term becomes uniform only at $M = 1/6$. When $M = 1/6$, the umklapp term is relevant for $K_+ < 4/9$. Then the ϕ_+ field is pinned and acquires a mass gap. This results in the $1/3$ -plateau phase with up-up-down spin structure. On the other hand, when approaching the $1/3$ -plateau from incommensurate magnetization $M \rightarrow 1/6$, K_+ takes the universal value $K_+ \rightarrow 2/9$.⁵⁷ This is a commensurate-incommensurate transition. Figure 7 indicates that the estimated decay exponent η at slightly above $M = 1/6$ seems smaller than $4/9$ even for $J_2/J_1 = 1.5$, suggesting the appearance of the $1/3$ -plateau at this coupling J_2/J_1 . This would mean that the upper critical value of the $1/3$ -plateau phase is larger than 1.5, $(J_2/J_1)_{p2} > 1.5$, which is larger than the previous estimate $(J_2/J_1)_{p2} \sim 1.25$ obtained from magnetization curves.²¹ While our estimated values of η may contain some large errors, another possible source of this discrepancy is that the analysis of magnetization curves could miss the plateau with an exponentially small width. Further studies with higher accuracy will be needed for resolving this issue.

V. 1/3-PLATEAU PHASE

The $1/3$ -plateau phase with a finite spin gap emerges at the magnetization $M = 1/6$ and for the parameter regime $0.487 < J_2/J_1 \lesssim 1.25$.^{21,36,37} In the $1/3$ -plateau

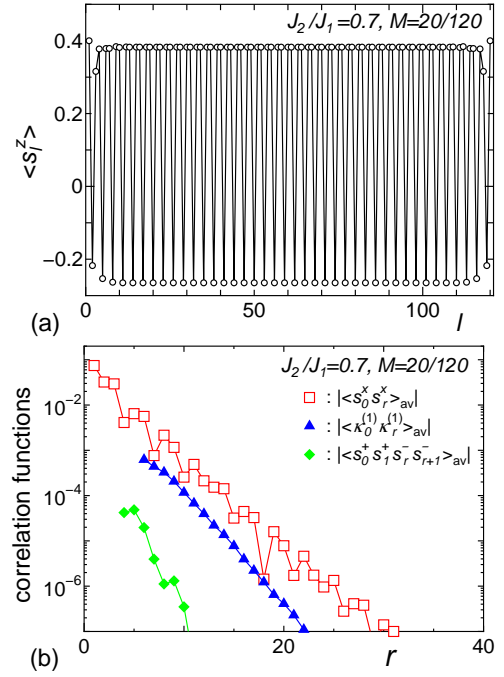


FIG. 8: (Color online) (a) Local magnetization $\langle s_l^z \rangle$ clearly shows the up-up-down spin configuration. (b) Semilog plot of the absolute values of the averaged correlation functions in the antiferromagnetic zigzag ladder with $L = 120$ spins for $(J_2/J_1, M) = (0.7, 20/120)$.

phase the system has the magnetic LRO of “up-up-down” structure,^{21,36} as shown in Fig. 8(a). The ground state is therefore three-fold degenerate in the thermodynamic limit.

The analysis of magnetization curves has shown that the $1/3$ -plateau phase is surrounded by the TLL1 and SDW_2 phases [see Fig. 1 of Ref. 21 and Fig. 1(b) of the present paper]. As we discussed in Secs. III and IV, we can understand this phase diagram as the $1/3$ -plateau phase emerging from instabilities of three-particle umklapp scattering processes which are inherent in the TLL1 and SDW_2 phases. Here we shall discuss how the up-up-down spin configuration emerges through pinning of bosonic fields.

When J_2/J_1 is small, the plateau emerges from the TLL1 phase. As discussed in Sec. III, the transition is induced by the three-particle umklapp scattering process. If we fix the magnetization at $M = 1/6$ and increase J_2/J_1 , the umklapp term becomes relevant at $K < 2/9$. Indeed we observed $K \simeq 2/9$ at $J_2/J_1 = 0.5$ in Fig. 4, which implies that for $J_2/J_1 \gtrsim 0.5$ the $1/3$ -plateau phase appears. As the umklapp term is relevant, the ϕ field is pinned at the bottom of the sine potential in Eq. (20), $\sqrt{4\pi}\langle\phi\rangle = \pi/2, 7\pi/6, 11\pi/6$ ($\lambda > 0$). The bosonization

formula of s_l^z , Eq. (8), then reduces to

$$\begin{aligned} s_l^z &= \frac{1}{6} - (-1)^l a \sin\left(\frac{\pi l}{3} + \sqrt{4\pi}\langle\phi\rangle\right) \\ &= \frac{1}{6} - a \cos\left(\frac{2\pi(l+n)}{3}\right), \quad (n=0,1,2), \end{aligned} \quad (35)$$

where $a > 0$. Equation (35) gives the up-up-down LRO with three-fold degeneracy in the ground state.^{67–69}

With larger J_2/J_1 , the plateau phase is next to the SDW₂ phase. As discussed in Sec. IV, this phase transition is controlled by the three-particle umklapp term, the second term in Eq. (34). When $K_+ < 4/9$ and $M = 1/6$, this term becomes relevant, and the ϕ_+ field is pinned to minimize the potential energy. The pinned values are $\sqrt{2\pi}\langle\phi_+\rangle = \pi/6, 5\pi/6, 3\pi/2$ ($\lambda < 0$). Substituting also $\phi_- = \langle\phi_- \rangle$ [Eq. (26)] into the bosonized form of s_l^z , Eq. (21), yields

$$s_l^z = \frac{1}{6} + a \sin\left(\frac{2\pi l}{3} + \sqrt{2\pi}\langle\phi_+\rangle\right), \quad (36)$$

which explains the three-fold-degenerate ground state with the up-up-down LRO.

Since both ϕ_+ and ϕ_- fields are pinned, all low-energy excitations in the 1/3-plateau phase are gapped. It thus follows that all correlation functions, except the long-ranged longitudinal spin correlation, decay exponentially. Figure 8 shows that the averaged correlation functions for $J_2/J_1 = 0.7$ and $M = 1/6$ as a typical example for the 1/3-plateau phase. The correlation functions decay exponentially in accordance with the theory.

VI. VECTOR CHIRAL PHASE

The vector chiral phase is characterized by the spontaneous breaking of parity symmetry accompanied by nonvanishing expectation value of the vector chirality, $\langle\kappa_l^{(n)}\rangle = \langle(\mathbf{s}_l \times \mathbf{s}_{l+n})^z\rangle \neq 0$. The bosonization theory for the vector chiral phase was developed in Refs. 32 and 41, and the appearance of the vector chiral LRO in the zigzag spin ladder (1) has been numerically confirmed recently.^{42,43} In this section we present results from our detailed numerical study of correlation functions and compare them with their asymptotic forms derived from the bosonization theory.

Let us first briefly summarize the results from the bosonization theory. As discussed in Sec. IV, the effective Hamiltonian (23) describes the zigzag spin ladder (1) in the limit $J_2 \gg J_1$. When the g_2 term is most relevant, we may employ the mean-field decoupling approximation³² in which both $d\theta_+/d\bar{x}$ and $\sin(\sqrt{2\pi}\theta_-)$ are assumed to acquire nonvanishing expectation values to minimize the g_2 term. The bosonic fields are thus pinned as

$$\langle\theta_-\rangle = \mp\sqrt{\frac{\pi}{8}}, \quad \left\langle\frac{d\theta_+}{d\bar{x}}\right\rangle = \pm\sqrt{\frac{2}{\pi}}c, \quad (37)$$

where c is a positive constant. Selecting one set of the signs from $(+, -)$ and $(-, +)$ in Eq. (37) corresponds to the spontaneous Z_2 -symmetry breaking in the vector chiral phase. The antisymmetric sector (ϕ_-, θ_-) thus acquires an energy gap and the low-energy physics of the phase is governed by the Gaussian model of the (ϕ_+, θ_+) fields, Eq. (27), in which the θ_+ field has been redefined as $\theta_+ \rightarrow \theta_+ - \langle d\theta_+/d\bar{x} \rangle \bar{x}$ to absorb the nonzero expectation value of $\langle d\theta_+/d\bar{x} \rangle$. The vector chiral phase is described by a one-component TLL theory defined by Eqs. (21), (22), (27), and (37).

Equation (22) allows us to write the vector chiral operators $\kappa_l^{(n)}$ as

$$\kappa_l^{(1)} \sim \sin(\sqrt{2\pi}\theta_-), \quad (38)$$

$$\kappa_l^{(2)} \sim \frac{d\theta_+}{d\bar{x}}. \quad (39)$$

The nonvanishing expectation values in Eq. (37) result in the vector chiral LRO in the ground state. We note that the expectation values of the vector chirality satisfy the relation

$$J_1\langle\kappa_l^{(1)}\rangle + 2J_2\langle\kappa_l^{(2)}\rangle = 0, \quad (40)$$

so that there is no net spin current.²² Furthermore, one can easily obtain the leading asymptotic behaviors of the transverse- and longitudinal-spin correlation functions as follows:

$$\langle s_0^x s_r^x \rangle = \frac{\tilde{A}^x}{|r|^{1/4K_+}} \cos(\tilde{Q}r) + \dots, \quad (41)$$

$$\langle s_0^x s_r^y \rangle = \pm \frac{\tilde{A}^x}{|r|^{1/4K_+}} \sin(\tilde{Q}r) + \dots, \quad (42)$$

$$\langle s_0^z s_r^z \rangle = M^2 - \frac{K_+}{\pi^2 r^2} + \dots, \quad (43)$$

where $\tilde{Q} = (\pi+c)/2$, and \tilde{A}^x is a positive constant. Equations (41) and (42) indicate that the spin components perpendicular to the applied field have a spiral structure with the incommensurate wavenumber \tilde{Q} , which comes from the finite expectation value of $\langle d\theta_+/d\bar{x} \rangle$. This helical quasi-LRO of the transverse components is a characteristic feature of the vector chiral phase. The sign factor \pm in Eq. (42) comes from the sign \pm in Eq. (37), and it defines the chirality, i.e., the direction of the spiral pitch. In the longitudinal-spin correlation function, the oscillating term with wavenumber $Q = \pi(\frac{1}{2} + M)$ decays exponentially as it includes the disordered ϕ_- field. Therefore, if $1/(4K_+) < 2$, the transverse-spin correlation function is dominant except the long-ranged vector chiral correlations.

In Fig. 9, we present our DMRG results of the averaged vector chiral correlation functions $\langle\kappa_0^{(n)}\kappa_r^{(n')}\rangle_{\text{av}}$ for $(J_2/J_1, M) = (1.2, 0.35)$, a representative point in the vector chiral phase. Clearly, the vector chiral correlations are long-range ordered (the reduction at $r > 100$ are due to boundary effects and should be ignored). Figure 10

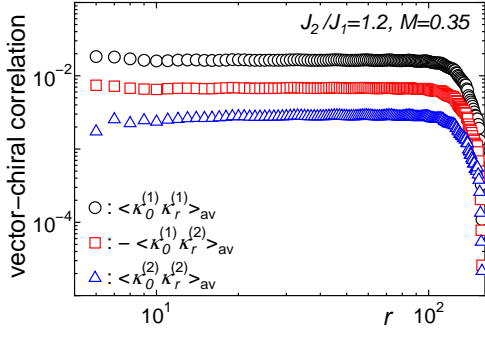


FIG. 9: (Color online) Averaged vector chiral correlation functions in the antiferromagnetic zigzag ladder with $L = 160$ spins for $(J_2/J_1, M) = (1.2, 0.35)$. Open circles, squares, and triangles respectively represent the DMRG data of $\langle \kappa_0^{(1)} \kappa_r^{(1)} \rangle_{av}$, $-\langle \kappa_0^{(1)} \kappa_r^{(2)} \rangle_{av}$, and $\langle \kappa_0^{(2)} \kappa_r^{(2)} \rangle_{av}$, where $\kappa_r^{(n)} = (\mathbf{s}_r \times \mathbf{s}_{r+n})^z$.

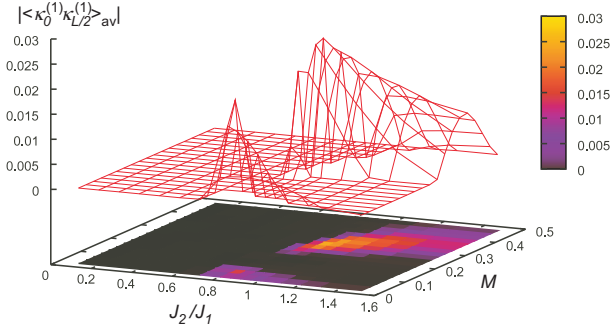


FIG. 10: (Color online) Amplitude of the vector chiral correlations at a distance $r = L/2$, $|\langle \kappa_0^{(1)} \kappa_{L/2}^{(1)} \rangle_{av}|$, in the antiferromagnetic zigzag ladder with $L = 160$ spins.

shows M and J_2/J_1 dependences of the amplitude of the vector chiral correlations measured at distance $r = L/2$, $|\langle \kappa_0^{(1)} \kappa_{L/2}^{(1)} \rangle_{av}|$, which indicates the strength of the LRO. This figure shows the parameter regions of the vector chiral phase; the parameter points where we observe the vector chiral LRO are plotted in Fig. 1(b). The vector chiral phase appears when J_2/J_1 is not small, and the phase space is split, by the SDW₂ phase, into two regions with either small or large magnetization M . This is in contrast with the J_1 - J_2 chain with ferromagnetic J_1 and AF J_2 which has the vector chiral phase only at small M .^{22,23,53} It is also important to note that each one of the vector chiral phases is next to a TLL2 phase [see Fig. 1(b)]. Incidentally, we have numerically confirmed that the vector chiral correlations satisfy the relation (40). These observations on the vector chiral order are consistent with the previous numerical results in Refs. 42 and 43.

To estimate the TLL parameter K_+ and the wavenumber \tilde{Q} of the spiral transverse-spin correlation, we fit the DMRG data of $\langle s_0^x s_r^x \rangle_{av}$ in the systems with $L = 120$

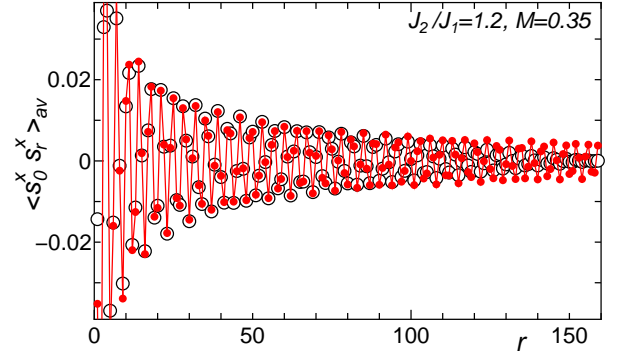


FIG. 11: (Color online) Averaged transverse-spin correlation function $\langle s_0^x s_r^x \rangle_{av}$ in the antiferromagnetic zigzag ladder with $L = 160$ spins for $(J_2/J_1, M) = (1.2, 0.35)$. Open circles represent the DMRG data. The fits to Eq. (41) are shown by solid red circles.

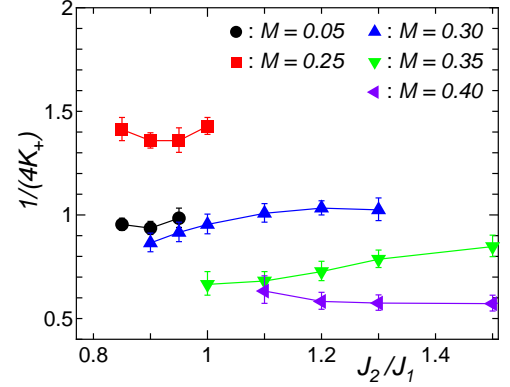


FIG. 12: (Color online) J_2/J_1 dependence of the decay exponent $1/(4K_+)$ of the transverse-spin correlation function $\langle s_0^x s_r^x \rangle_{av}$ in the vector chiral phase for the antiferromagnetic zigzag ladder with $L = 160$ sites.

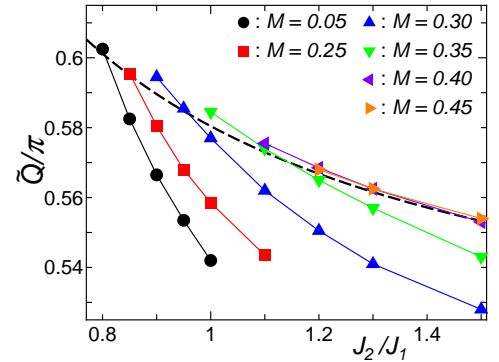


FIG. 13: (Color online) J_2/J_1 dependence of the wavenumber \tilde{Q} of the transverse-spin correlation function $\langle s_0^x s_r^x \rangle_{av}$ in the vector chiral phase for the antiferromagnetic zigzag ladder with $L = 160$ sites. The dashed curve represent the classical pitch angle $\tilde{Q} = \arccos(-J_1/4J_2)$.

and 160 spins to Eq. (41), with taking \tilde{Q} , K_+ , and \tilde{A}^x as fitting parameters. Figure 11 shows the result for $(J_2/J_1, M) = (1.2, 0.35)$ and $L = 160$. We see that the DMRG data are fitted very well to the analytic form, except for large distances $r \gtrsim 100$ where the boundary effect is not negligible. The good agreement between the numerical data and the fits supports the validity of the TLL theory for the vector chiral phase.

The decay exponent $1/(4K_+)$ of the transverse-spin correlation $\langle s_0^x s_r^x \rangle_{\text{av}}$ is shown in Fig. 12. We have compared the estimates from $L = 160$ and 120 spins and confirmed that the finite-size effect is negligible in the data shown in the figure but not so for some parameter points (results for which are not shown in Fig. 12) in the very vicinity of the phase boundaries. It turns out that the exponent is rather small, $1/(4K_+) \lesssim 1$, in most parameter region of the vector chiral phase, suggesting the dominant spiral transverse-spin correlation. The exponent becomes larger, as we move closer to the $1/3$ -plateau phase.

Figure 13 shows the wavenumber \tilde{Q} of the transverse-spin correlation function. While \tilde{Q} almost coincides with the classical pitch angle $\arccos(-J_1/4J_2)$ near the boundary to the TLL2 phase, it becomes smaller than the classical pitch angle with increasing J_2/J_1 , i.e., moving inside the vector chiral phase. We thus find that the incommensurate wavenumber \tilde{Q} in the vector chiral phase is renormalized towards the commensurate value $\pi/2$ due to quantum fluctuations.

VII. TLL2 PHASE

The TLL2 phase is a two-component TLL consisting of two flavors of free bosons. In this section, we develop its effective low-energy theory based on the bosonization of Jordan-Wigner fermions. We then discuss DMRG results, which support the effective theory.

The TLL2 phase is realized in two separated regions of high and low magnetic fields in the magnetic phase diagram. Here we first consider the high-field TLL2 phase, for which the origin of the two bosonic modes can be easily understood by examining the instability of the ferromagnetic phase.

Inside the ferromagnetic phase ($h > h_s$), the spin-wave excitation has a finite energy gap and the dispersion relation is given by Eq. (6). As the magnetic field is lowered, the energy gap decreases and vanishes at the saturation field $h = h_s$. For $h < h_s$, the soft magnons proliferate and collectively form a TLL. We notice that there are two distinct cases:

(i) When $J_2/J_1 < 1/4$, the bottom of the single-magnon dispersion is at $k = \pi \pmod{2\pi}$. Magnons with $k \approx \pi$ become soft and condense below the saturation field h_s , yielding a one-component TLL. Indeed, we have found the TLL1 phase in this case (see Sec. III).

(ii) When $J_2/J_1 > 1/4$, the dispersion has two minima, $k = \pi \pm Q_0$ with $Q_0 = \arccos(J_1/4J_2)$. Both magnons

with $k = \pi + Q_0$ and $\pi - Q_0$ become soft and proliferate below the saturation field. The resulting phase is the TLL2 phase which consists of equal densities of two flavors of condensed magnons. We note that, if the densities are not equal, the vector chiral phase will be realized,⁴¹ as we will discuss later.

A similar argument should apply to the TLL2 phase appearing at lower magnetic field. The elementary excitation driving the instability of the dimer ground state is a “spinon,” a domain wall separating two regions of different dimer pattern.^{74–76} For $J_2/J_1 < (J_2/J_1)_L$, the dispersion of the two-spinon state has a single minimum at $k = \pi$ and only one soft mode is relevant in destabilizing the dimer state. The TLL1 phase is thus expected to show up for $M > 0$. For $J_2/J_1 > (J_2/J_1)_L$, on the other hand, the two-spinon excitation spectrum exhibits a double-well structure with minima at incommensurate momenta $k = \pm k_0$, which leads to the TLL2 (or vector chiral) phase for $M > 0$. The critical coupling at which the lowest points deviate from $k = \pi$ has been estimated to be $(J_2/J_1)_L = 0.54$.⁷⁶

A. Two-component TLL theory

In this subsection we describe the two-component TLL theory of the high-field TLL2 phase in detail. As we discussed above, this phase can be understood as a two-component TLL emerging from condensation of two soft magnon modes. This suggests to formulate a low-energy effective theory in terms of interacting magnons.^{41,72} Such an approach is valid and useful near the saturation field. An alternative approach we adopt here is to formulate the low-energy theory in terms of Jordan-Wigner fermions filling two separate Fermi seas. Advantage of the latter approach is that it can be applied in the whole TLL2 phase. The connection to the magnon picture will also be discussed below.

We apply the Jordan-Wigner transformation

$$s_l^z = \frac{1}{2} - f_l^\dagger f_l, \quad (44a)$$

$$s_l^+ = (-1)^l f_l \exp \left(-i\pi \sum_{n<l} f_n^\dagger f_n \right), \quad (44b)$$

$$s_l^- = (-1)^l f_l^\dagger \exp \left(i\pi \sum_{n<l} f_n^\dagger f_n \right), \quad (44c)$$

to rewrite the Hamiltonian (1) in the form $H = H_0 + H'$, where

$$\begin{aligned} H_0 = & -\frac{J_1}{2} \sum_l \left(f_l^\dagger f_{l+1} + f_{l+1}^\dagger f_l \right) \\ & + J_2 M \sum_l \left(f_l^\dagger f_{l+2} + f_{l+2}^\dagger f_l \right) \\ & - [2M(J_1 + J_2) - h] \sum_l f_l^\dagger f_l, \end{aligned} \quad (45)$$

and

$$\begin{aligned}
H' = & J_1 \sum_l :f_l^\dagger f_l :: f_{l+1}^\dagger f_{l+1} : \\
& + J_2 \sum_l \left(:f_l^\dagger f_l :: f_{l+2}^\dagger f_{l+2} : - f_{l+2}^\dagger f_l : f_{l+1}^\dagger f_{l+1} : \right. \\
& \left. - f_l^\dagger f_{l+2} : f_{l+1}^\dagger f_{l+1} : \right). \quad (46)
\end{aligned}$$

Here $:X:$ denotes normal ordering of X with respect to the filled Fermi sea of fermions with the dispersion

$$E(k) = -J_1 \cos k + 2J_2 M \cos(2k) - 2M(J_1 + J_2) + h, \quad (47)$$

determined from Eq. (45). Note that the wave number k is measured from π as the $(-1)^l$ factor is included in the Jordan-Wigner transformation. As discussed above, in the TLL2 phase the dispersion has two minima and, accordingly, there are four Fermi points located at $k = \pm k_s, \pm k_l$ ($k_s < k_l$, see Fig. 14). The density of fermions is

$$\rho = \frac{1}{\pi}(k_l - k_s) = \frac{1}{2} - M. \quad (48)$$

In the limit $M \rightarrow \frac{1}{2}$, both k_l and k_s approach Q_0 . Introducing slowly-varying fermionic fields for each Fermi point, we write the fermion annihilation operator as

$$\begin{aligned}
f_j = & e^{ik_l x} \psi_{lR}(x) + e^{-ik_l x} \psi_{lL}(x) \\
& + e^{ik_s x} \psi_{sL}(x) + e^{-ik_s x} \psi_{sR}(x), \quad (49)
\end{aligned}$$

where the continuous variable x is identified lattice index j . We linearize the dispersion around the four Fermi points and replace H_0 with

$$\begin{aligned}
\tilde{H}_0 = & iv_l \int dx \left(\psi_{lL}^\dagger \frac{d}{dx} \psi_{lL} - \psi_{lR}^\dagger \frac{d}{dx} \psi_{lR} \right) \\
& + iv_s \int dx \left(\psi_{sL}^\dagger \frac{d}{dx} \psi_{sL} - \psi_{sR}^\dagger \frac{d}{dx} \psi_{sR} \right), \quad (50)
\end{aligned}$$

where the velocities v_l and v_s are in general different. The linearized kinetic term can be written as

$$\tilde{H}_0 = \sum_{\nu=l,s} \frac{v_\nu}{4\pi} \int dx \left[\left(\frac{d\varphi_{\nu L}}{dx} \right)^2 + \left(\frac{d\varphi_{\nu R}}{dx} \right)^2 \right] \quad (51)$$

in terms of the chiral bosonic fields $\varphi_{\nu L}$ and $\varphi_{\nu R}$, which obey the commutation relations

$$\begin{aligned}
[\varphi_{\nu R}(x), \varphi_{\nu R}(y)] &= i\pi \text{sgn}(x-y), \\
[\varphi_{\nu L}(x), \varphi_{\nu L}(y)] &= -i\pi \text{sgn}(x-y), \\
[\varphi_{\nu R}(x), \varphi_{\nu',L}(y)] &= -i\pi \delta_{\nu,\nu'}. \quad (52)
\end{aligned}$$

The fermion densities are written as

$$\begin{aligned}
\rho_{\nu R}(x) &= : \psi_{\nu R}^\dagger(x) \psi_{\nu R}(x) : = \frac{1}{2\pi} \frac{d\varphi_{\nu R}}{dx}, \\
\rho_{\nu L}(x) &= : \psi_{\nu L}^\dagger(x) \psi_{\nu L}(x) : = \frac{1}{2\pi} \frac{d\varphi_{\nu L}}{dx}. \quad (53)
\end{aligned}$$

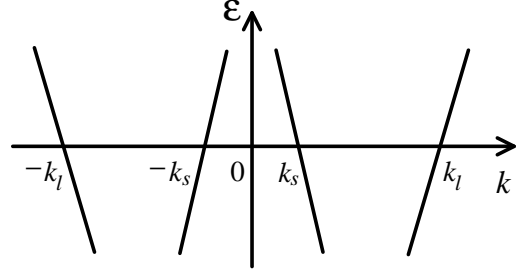


FIG. 14: Four Fermi points located at $k = \pm k_s$ and $\pm k_l$. The density of fermions is related to the magnetization, $k_l - k_s = \pi(\frac{1}{2} - M)$. The phase transition to the TLL1 phase occurs when $k_s = 0$, i.e., when the inner two Fermi points merge at $k = 0$.

Finally, the slowly-varying fermionic fields are bosonized,

$$\begin{aligned}
\psi_{\nu R}(x) &= \frac{\eta_\nu}{\sqrt{2\pi\alpha}} e^{i\varphi_{\nu R}(x)}, \\
\psi_{\nu L}(x) &= \frac{\eta_\nu}{\sqrt{2\pi\alpha}} e^{-i\varphi_{\nu L}(x)}, \quad (54)
\end{aligned}$$

where α is a short-distance cutoff of the order of the lattice spacing, and η_ν are the Klein factors obeying $\{\eta_\nu, \eta_{\nu'}\} = 2\delta_{\nu,\nu'}$.

The interaction Hamiltonian H' gives rise to various scattering processes of fermionic fields $\psi_{\nu L/R}$. Among all, important in the TLL2 phase are (short-range) density-density interactions,

$$\begin{aligned}
H_\rho = & \pi \int dx \{ 2g_{2l} \rho_{lL}(x) \rho_{lR}(x) + 2g_{2s} \rho_{sL}(x) \rho_{sR}(x) \\
& + 2g_{2\perp} [\rho_{lL}(x) \rho_{sR}(x) + \rho_{lR}(x) \rho_{sL}(x)] \\
& + g_{4l} [\rho_{lL}(x) \rho_{lL}(x) + \rho_{lR}(x) \rho_{lR}(x)] \\
& + g_{4s} [\rho_{sL}(x) \rho_{sL}(x) + \rho_{sR}(x) \rho_{sR}(x)] \\
& + 2g_{4\perp} [\rho_{lL}(x) \rho_{sL}(x) + \rho_{lR}(x) \rho_{sR}(x)] \}, \quad (55)
\end{aligned}$$

where $g_{2l/s}$, $g_{2\perp}$, $g_{4l/s}$, and $g_{4\perp}$ are coupling constants that depend on J_1 , J_2 , and M . We define the phase fields ($\nu = l, s$)

$$\begin{aligned}
\phi_\nu(x) &= \frac{1}{\sqrt{4\pi}} [\varphi_{\nu L}(x) + \varphi_{\nu R}(x)], \\
\theta_\nu(x) &= \frac{1}{\sqrt{4\pi}} [\varphi_{\nu L}(x) - \varphi_{\nu R}(x)]. \quad (56)
\end{aligned}$$

The effective Hamiltonian $H_2 = \tilde{H}_0 + H_\rho$ is then quadratic in ϕ_ν and θ_ν , and is diagonalized as

$$H_2 = \int dx \sum_{\mu=\pm} \frac{v_\mu}{2} \left[\left(\frac{d\theta_\mu}{dx} \right)^2 + \left(\frac{d\phi_\mu}{dx} \right)^2 \right] \quad (57)$$

by the new fields θ_\pm and ϕ_\pm which are linearly related to $\theta_{l,s}$ and $\phi_{l,s}$ by

$$\begin{pmatrix} \phi_l \\ \phi_s \end{pmatrix} = A^T \begin{pmatrix} \phi_+ \\ \phi_- \end{pmatrix}, \quad \begin{pmatrix} \theta_l \\ \theta_s \end{pmatrix} = A^{-1} \begin{pmatrix} \theta_+ \\ \theta_- \end{pmatrix}. \quad (58)$$

Here the 2×2 matrix

$$A = \begin{pmatrix} A_{11} & A_{12} \\ A_{21} & A_{22} \end{pmatrix} \quad (59)$$

is a function of the velocities $v_{l,s}$ and the coupling constants g 's, whose functional form can be found in Ref. 71. Without loss of generality, we can assume $v_+ > v_-$.

The Hamiltonian H_2 (57) is the low-energy effective theory of the TLL2 phase. It consists of two free bosonic sectors (ϕ_+, θ_+) and (ϕ_-, θ_-) . Other interactions which are not included in H_ρ are irrelevant perturbations to H_2 in the TLL2 phase. An important example of such interactions is the backward-scattering interaction

$$\begin{aligned} H_b &= g_{1\perp} \int dx \left[\psi_{sL}^\dagger(x) \psi_{sR}^\dagger(x) \psi_{lL}(x) \psi_{lR}(x) + \text{H.c.} \right] \\ &= -\frac{g_{1\perp}}{2\pi^2\alpha^2} \int dx \cos[\sqrt{4\pi}(\theta_l - \theta_s)]. \end{aligned} \quad (60)$$

The irrelevance of the operator $\cos[\sqrt{4\pi}(\theta_l - \theta_s)]$ imposes the condition

$$\frac{1}{(\det A)^2} [(A_{11} + A_{12})^2 + (A_{21} + A_{22})^2] > 2. \quad (61)$$

We note that the vertex operators $\exp(\pm i\sqrt{4\pi}\phi_\pm)$ and $\exp(\pm i\sqrt{4\pi}\theta_\pm)$ have scaling dimension 1.

The matrix A takes a simple form

$$A = \frac{1}{\sqrt{2}} \begin{pmatrix} \sqrt{K_+} & 0 \\ 0 & \sqrt{K_-} \end{pmatrix} \begin{pmatrix} 1 & 1 \\ 1 & -1 \end{pmatrix}, \quad (62)$$

when the two conditions

$$v_l + g_{4l} = v_s + g_{4s} =: v + g_4, \quad (63a)$$

$$g_{2l} = g_{2s} =: g_2, \quad (63b)$$

are satisfied. In this case, the TLL parameters K_\pm and the renormalized velocities v_\pm are given by

$$K_\pm = \left(\frac{v + g_4 \pm g_{4\perp} - g_2 \mp g_{2\perp}}{v + g_4 \pm g_{4\perp} + g_2 \pm g_{2\perp}} \right)^{1/2}, \quad (64a)$$

$$v_\pm = [(v + g_4 \pm g_{4\perp})^2 - (g_2 \pm g_{2\perp})^2]^{1/2}. \quad (64b)$$

This simplified effective theory is applicable when $J_2/J_1 \gg 1/4$ and $|M - \frac{1}{2}| \ll \frac{1}{2}$, i.e., when the magnon density is very low and $k_l - k_s \ll k_s$. In this case one can build an effective theory by treating magnons with $k = \pi \pm Q_0$ as interacting hard-core bosons.^{41,72} We adopt a phenomenological effective Hamiltonian of interacting bosons ($0 < v < u$),⁸¹

$$\begin{aligned} H_B &= \int dx \left[\frac{1}{2m} \left(\frac{d\psi_+^\dagger}{dx} \frac{d\psi_+}{dx} + \frac{d\psi_-^\dagger}{dx} \frac{d\psi_-}{dx} \right) \right. \\ &\quad \left. + u \{ [\rho_+(x)]^2 + [\rho_-(x)]^2 \} + 2v\rho_+(x)\rho_-(x) \right], \end{aligned} \quad (65)$$

where $\psi_\pm(x)$ are field operators of two flavors of magnons satisfying $[\psi_\mu(x), \psi_{\mu'}^\dagger(y)] = \delta_{\mu,\mu'}\delta(x-y)$, magnon density fluctuations $\rho_\pm(x) = \psi_\pm^\dagger(x)\psi_\pm(x) - \rho/2$, and m is their effective mass. The boson density (per flavor) is assumed to be $\rho/2$, where ρ is defined in Eq. (48). In the low-energy, hydrodynamic limit,^{46,73} the magnon fields and density fluctuations are written as

$$\psi_\pm(x) \sim \sqrt{\frac{\rho}{2}} e^{i\vartheta_\pm(x)} + \dots, \quad (66a)$$

$$\rho_\pm(x) \sim \frac{1}{\pi} \frac{d\varphi_\pm(x)}{dx} + \rho \cos[\pi\rho x + 2\varphi_\pm(x)] + \dots, \quad (66b)$$

where the phase fields obey $[\varphi_\mu(x), \partial_y \vartheta_{\mu'}(y)] = i\pi\delta_{\mu,\mu'}\delta(x-y)$. Substituting (66) into (65) yields

$$\begin{aligned} H_B &= \int dx \left\{ \frac{\rho}{4m} \left[\left(\frac{d\vartheta_+}{dx} \right)^2 + \left(\frac{d\vartheta_-}{dx} \right)^2 \right] \right. \\ &\quad \left. + \frac{u}{\pi^2} \left[\left(\frac{d\varphi_+}{dx} \right)^2 + \left(\frac{d\varphi_-}{dx} \right)^2 \right] \right. \\ &\quad \left. + \frac{2v}{\pi^2} \frac{d\varphi_+}{dx} \frac{d\varphi_-}{dx} + v\rho^2 \cos[2(\varphi_+ - \varphi_-)] \right\}. \end{aligned} \quad (67)$$

Once we make the identification of the phase fields,

$$\varphi_+ = \frac{1}{2}(\varphi_{sL} + \varphi_{lR}), \quad \vartheta_+ = \frac{1}{2}(\varphi_{sL} - \varphi_{lR}), \quad (68a)$$

$$\varphi_- = \frac{1}{2}(\varphi_{lL} + \varphi_{sR}), \quad \vartheta_- = \frac{1}{2}(\varphi_{lL} - \varphi_{sR}), \quad (68b)$$

we can readily see that the Hamiltonian (67) is a special case of $\tilde{H}_0 + H_\rho + H_b$, with the coupling constants,

$$v_l + g_{4l} = v_s + g_{4s} = \frac{\pi\rho}{4m} + \frac{u}{\pi}, \quad (69a)$$

$$g_{2l} = g_{2s} = g_{4\perp} = \frac{v}{\pi}, \quad (69b)$$

$$g_{2\perp} = -\frac{\pi\rho}{4m} + \frac{u}{\pi}. \quad (69c)$$

Substituting (69) into (64), we find

$$v_\pm = \sqrt{\frac{\rho}{m}(u \pm v)}, \quad (K_\pm)^{\pm 1} = \frac{\pi}{2} \sqrt{\frac{\rho}{m(u \pm v)}}. \quad (70)$$

Note that v_- and K_- vanish when $u = v$. This corresponds to the instability to the vector chiral order.^{41,72,81,82} We emphasize again that the bosonic approach described here is applicable only when $\frac{1}{2} - M \ll 1$ and $J_2/J_1 \gg 1/4$, while the general theory (57)–(58) should be valid as a low-energy theory in the whole TLL2 phase.

Next we express the spin operators \mathbf{s}_l using the phase fields in the fermionic formulation. We first rewrite the string operator used in the Jordan-Wigner transformation,

$$\begin{aligned} \exp \left(i\pi \sum_{n<l} f_n^\dagger f_n \right) &= e^{i(k_l - k_s)x + i\sqrt{\pi}[\phi_l(x^-) + \phi_s(x^-)]} \\ &\quad + e^{-i(k_l - k_s)x - i\sqrt{\pi}[\phi_l(x^-) + \phi_s(x^-)]}, \end{aligned} \quad (71)$$

where $x^- = x - 0^+$, and the second term is added to ensure the Hermiticity of the string operator. From Eqs. (44c), (49) (54), and (71), we obtain

$$\begin{aligned} s_l^- = & (-1)^x \eta_s e^{i\sqrt{\pi}\theta_s(x)} \cos[k_l x + \sqrt{\pi}\phi_l(x)] \\ & + (-1)^x \eta_l e^{i\sqrt{\pi}\theta_l(x)} \cos[-k_s x + \sqrt{\pi}\phi_s(x)] \\ & + (-1)^x \eta_s e^{i\sqrt{\pi}\theta_s} \cos[(k_l - 2k_s)x + \sqrt{\pi}(\phi_l + 2\phi_s)] \\ & + (-1)^x \eta_l e^{i\sqrt{\pi}\theta_l} \cos[(2k_l - k_s)x + \sqrt{\pi}(2\phi_l + \phi_s)] \\ & + \dots, \end{aligned} \quad (72)$$

where numerical coefficients are suppressed for simplicity. The transverse correlation function becomes

$$\langle s_0^+ s_r^- \rangle = \frac{(-1)^r c_l}{r^{x_l}} \cos(k_l r) + \frac{(-1)^r c_s}{r^{x_s}} \cos(k_s r) + \dots, \quad (73)$$

where c_l and c_s are constants, and the exponents are given by

$$\begin{aligned} x_l &= \frac{1}{2}(A_{11}^2 + A_{21}^2) \left[1 + \frac{1}{(\det A)^2} \right], \\ x_s &= \frac{1}{2}(A_{12}^2 + A_{22}^2) \left[1 + \frac{1}{(\det A)^2} \right]. \end{aligned} \quad (74)$$

It follows from $s_l^z = \frac{1}{2} - s_l^- s_l^+$ that

$$\begin{aligned} s_l^z = & M - \frac{1}{\sqrt{\pi}} \frac{d}{dx} (\phi_l + \phi_s) \\ & + c_1 \sin(2k_l x + \sqrt{4\pi}\phi_l) + c_2 \sin(-2k_s x + \sqrt{4\pi}\phi_s) \\ & + c_3 \cos[(k_l - k_s)x + \sqrt{\pi}(\phi_l + \phi_s)] \sin[\sqrt{\pi}(\theta_l - \theta_s)] \\ & + c_4 \cos[(k_l + k_s)x + \sqrt{\pi}(\phi_l - \phi_s)] \sin[\sqrt{\pi}(\theta_l - \theta_s)] \\ & + c_5 \cos[2(k_l - k_s)x + \sqrt{4\pi}(\phi_l + \phi_s)] \\ & + c_6 \cos[2(2k_l - k_s)x + \sqrt{4\pi}(2\phi_l + \phi_s)] + \dots, \end{aligned} \quad (75)$$

where c_j 's are nonuniversal constants. The long-distance behavior of the longitudinal spin correlation is then obtained as

$$\begin{aligned} \langle s_0^z s_r^z \rangle = & M^2 - \frac{1}{2\pi^2 r^2} [(A_{11} + A_{12})^2 + (A_{21} + A_{22})^2] \\ & + \frac{C_1}{r^{x_1}} \cos(2k_l r) + \frac{C_2}{r^{x_2}} \cos(2k_s r) \\ & + \frac{C_3}{r^{x_3}} \cos[(k_l - k_s)r] + \frac{C_4}{r^{x_4}} \cos[(k_l + k_s)r] \\ & + \frac{C_5}{r^{x_5}} \cos[2(k_l - k_s)r] + \frac{C_6}{r^{x_6}} \cos[2(2k_l - k_s)r] \\ & + \dots, \end{aligned} \quad (76)$$

where C_j 's are constants, and the exponents are given by

$$\begin{aligned} x_1 &= 2(A_{11}^2 + A_{21}^2), & x_2 &= 2(A_{12}^2 + A_{22}^2), \\ x_3 &= \frac{1}{2}[(A_{11} + A_{12})^2 + (A_{21} + A_{22})^2] \left[1 + \frac{1}{(\det A)^2} \right], \\ x_4 &= \frac{1}{2}[(A_{11} - A_{12})^2 + (A_{21} - A_{22})^2] \\ &\quad + \frac{1}{2(\det A)^2} [(A_{11} + A_{12})^2 + (A_{21} + A_{22})^2], \\ x_5 &= 2[(A_{11} + A_{12})^2 + (A_{21} + A_{22})^2], \\ x_6 &= 2[(2A_{11} + A_{12})^2 + (2A_{21} + A_{22})^2]. \end{aligned} \quad (77)$$

Finally, let us consider local spin polarization $\langle s_l^z \rangle$ near an open boundary of a semi-infinite spin chain defined on the sites $l > 0$. Assuming the Dirichlet boundary conditions $\phi_l(0) = \phi_s(0) = 0$ as in the TLL1 phase [see Eq. (15)], we obtain

$$\begin{aligned} \langle s_l^z \rangle = & M + \frac{c_1}{(2l)^{x_1/2}} \sin(2k_l l) - \frac{c_2}{(2l)^{x_2/2}} \sin(2k_s l) \\ & + \frac{c_5}{(2l)^{x_5/2}} \cos[2(k_l - k_s)l] \\ & + \frac{c_6}{(2l)^{x_6/2}} \cos[2(2k_l - k_s)l] + \dots \end{aligned} \quad (78)$$

Observe that the exponents in Eq. (78) are a half of the corresponding ones in Eq. (76) and that the vertex operators of the $\theta_{l,s}$ fields do not contribute to Eq. (78).

An important characteristic feature of the spin correlations (73) and (76) in the TLL2 phase is the presence of two incommensurate (Fermi) wave numbers k_l and k_s (and their linear combinations).

Before closing this subsection, we note that Frahm and R odenbeck studied an exactly solvable zigzag spin ladder model with additional three-spin interactions.^{77,78} Their model has a phase corresponding to our TLL2 phase. They have calculated, using the Bethe ansatz solution and conformal field theory, exponents of several terms in the longitudinal spin correlation (76).

B. Instabilities

In the magnetic phase diagram (Fig. 1) each TLL2 phase is next to a vector chiral phase and the TLL1 phase. Since these neighboring phases are one-component TLLs, one of the two massless modes in the low-energy Hamiltonian (57) has to become massive or disappear from low-energy spectra at the transitions from the TLL2 phase. Here we discuss instabilities of gapless modes in the TLL2 phases which cause the phase transitions to the vector chiral and TLL1 phases.

As pointed out by Kolezhuk and Vekua,⁴¹ in the interacting magnon picture valid in the vicinity of the saturation field [Eqs. (65)–(70)], the instability to the vector chiral phase corresponds to the “demixing” or “phase separation” instability,^{81,82} which occurs when both v_-

and K_- vanish. Alternatively, if we regard the two flavors as up and down pseudospins, the TLL2 and vector chiral phases correspond to paramagnetic and ferromagnetic phases, respectively. The transition between the TLL2 and vector chiral phases is then regarded as a ferromagnetic transition.⁸³ Away from the saturation field, the interacting magnon picture is no longer applicable, and we should use the low-energy effective Hamiltonian (57) with the A matrix (59). The instability to the vector chiral phase is then signaled by $v_- = 0$ and $\det A = 0$.

The transition between the TLL2 and TLL1 phases is characterized by a cusp singularity in the magnetization curve.²¹ Since M and h correspond to the particle density and the chemical potential of the Jordan-Wigner fermions, the origin of the cusp singularity can be attributed to the van Hove singularity of the fermion density of states, which exists at the saddle point $k = 0$ of the dispersion (47). Thus, the TLL2-TLL1 transition is considered to occur when the chemical potential matches the saddle-point energy, and the two Fermi seas merge into a single Fermi sea.³⁵ Indeed, the Bethe-ansatz study of a solvable model finds that the transition of commensurate-incommensurate type occurs when $k_s = 0$.^{77,78} In our low-energy effective theory, the transition is driven by the operator (the c_2 term in s_l^z),

$$\tilde{h} \int dx \sin(-2k_s x + \sqrt{4\pi}\phi_s), \quad (79)$$

which turns into a mass term (scaling dimension 1) for fermions at the TLL2-TLL1 transition. Comparison of our effective theory with the Bethe-ansatz study in Ref. 78 shows that the A matrix takes the form

$$A = \begin{pmatrix} \xi(\Lambda_2) & 0 \\ -1 + \xi(0) & 1 \end{pmatrix}, \quad (80)$$

at the transition ($h \searrow h_{c1}$), in agreement with our picture of the TLL2-TLL1 transition as a commensurate-incommensurate transition caused by the operator (79). Here ξ is the dressed charge defined in Ref. 78.

C. Numerical results

In Fig. 2(e) we have shown the correlation functions at $J_2/J_1 = 0.6$ and $M = 0.4$, as a typical example of the TLL2 phase. We see that both the longitudinal- and transverse-spin correlation functions decay algebraically. The vector chiral LRO is clearly absent.

As we have discussed in Sec. VII A, the defining feature of the TLL2 phase is that its low-energy physics is governed by the two independent set of free bosons. The low-energy theory is a conformal field theory with central charge $c = 1 + 1$. The central charge can be numerically measured through the entanglement entropy,

$$S(l) = -\text{Tr}_\Omega [\rho(l) \ln \rho(l)], \quad (81)$$

where the reduced density matrix for the subsystem $\Omega = \{s_j | 1 \leq j \leq l\}$ is defined by

$$\rho(l) = \text{Tr}_{\bar{\Omega}} |0\rangle\langle 0|. \quad (82)$$

Here $|0\rangle$ is the ground state wave function, and the spins s_{l+1}, \dots, s_L in the environment $\bar{\Omega}$ are traced out. The entanglement entropy of a 1D critical system is known to have a logarithmic dependence on l ,⁸⁴⁻⁸⁶

$$S(l) = \frac{c}{6} \ln l + \text{const.}, \quad (83)$$

in the open chain in the thermodynamic limit, $L \rightarrow \infty$ and $l \gg 1$. For finite-size systems of L spins, $\ln l$ in Eq. (83) should be replaced by⁸⁵

$$x = \ln \left[\frac{L}{\pi} \sin \left(\frac{\pi l}{L} \right) \right]. \quad (84)$$

Hence we can measure the central charge c as a coefficient of x . This method was recently used to detect the central charge of the critical spin Bose metal phase in a related model of the J_1 - J_2 zigzag ladder with a ring exchange interaction.⁸⁷ Figure 15(a) shows the entanglement entropy $S(l)$ in the TLL2 phase ($J_2/J_1 = 0.6$, $M = 0.4$) as a function of x . We clearly see that $S(l) \sim x/3$, indicating that $c = 2$. For comparison, we have computed the entanglement entropy in the TLL1 and vector chiral phases. The numerical results shown in Fig. 15(b) demonstrate that $S(l) \sim x/6$ for large x , i.e., $c = 1$.

Having confirmed that the TLL2 phase has $c = 2$, i.e., that the low-energy physics is governed by two free boson theories, we now discuss spin correlation functions. It turned out, however, that the presence of the two Fermi wavenumbers k_l and k_s makes it difficult to analyze correlation functions in the TLL2 phase. For this reason we focus attention to the simplest, one-point function $\langle s_l^z \rangle$. The Friedel oscillations near open boundaries give us information on the Fermi wavenumbers.

We show in Figs. 16 and 17 the squared modulus of the Fourier transform of the local spin polarization

$$s^z(k) = \frac{1}{\sqrt{L}} \sum_{l=1}^L e^{ikl} (\langle s_l^z \rangle - M). \quad (85)$$

At $J_2/J_1 = 0.6$ (Fig. 16) the TLL2 phases appear when $0 < M \lesssim 0.075$ and $0.25 \lesssim M < 1/2$, and the TLL1 phase is located at $0.1 \lesssim M \lesssim 0.2$. In the TLL1 phase we see a very sharp peak in $|s^z(k)|^2$ at $k = \pi(1 - 2M)$, in agreement with Eq. (15). Although greatly reduced in magnitude, the peak persists in the TLL2 phases. This faint peak comes from the fourth term, with wavenumber $2(k_l - k_s)$, in Eq. (78). We attribute the strongest peak of $|s^z(k)|^2$ in the TLL2 phase to the second term in Eq. (78) with wavenumber $2k_l$. The two peaks meet when the TLL2 phase is turned into the TLL1 phase, i.e., when k_s vanishes, in accordance with the discussion in Sec. VII B. Moreover, at the saturation limit $M \rightarrow 1/2$, the wavenumber k_{max} of the strongest peak

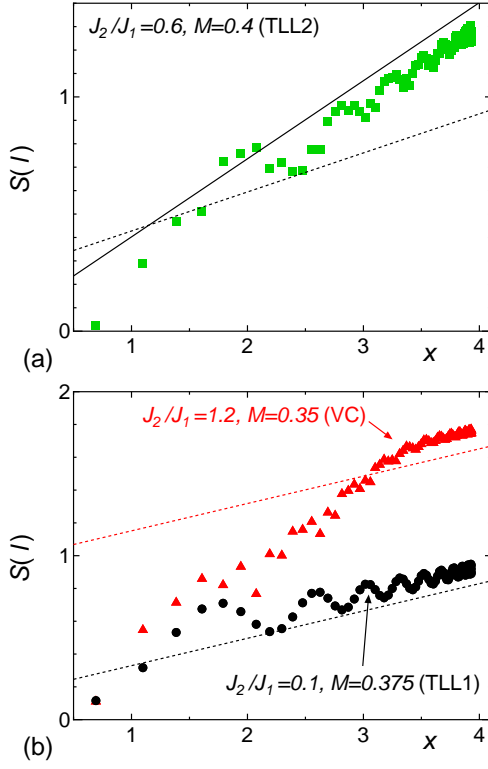


FIG. 15: (Color online) (a) Entanglement entropy of the TLL2 phase ($J_2/J_1 = 0.6$, $M = 0.4$). The horizontal axis is $x = \ln[(L/\pi) \sin(\pi l/L)]$. Solid and dotted lines represent the slope $1/3$ ($c = 2$) and $1/6$ ($c = 1$), respectively. (b) Entanglement entropy of the TLL1 phase ($J_2/J_1 = 0.1$, $M = 0.375$) and the vector chiral phase ($J_2/J_1 = 1.2$, $M = 0.35$). Dotted lines indicate the slope $1/6$ ($c = 1$).

approaches $2Q_0 = 2 \arccos(J_1/4J_2)$, where Q_0 is the momentum of the soft magnon in the ferromagnetic state, while $k_{\max} \rightarrow 2k_0$ as $M \rightarrow 0$, where k_0 is the momentum of the soft single-spinon excitation in the dimer phase estimated numerically.⁷⁶ In the higher-field TLL2 phase we see a third, faint peak, whose wavenumber k_3 equals $2Q_0$ at $M \rightarrow 1/2$ and increases with decreasing M . We have found numerically that $k_3 - k_{\max}$ equals $2(k_l - k_s) = \pi(1 - 2M)$ modulo 2π , from which we conclude $k_3 = 4k_l - 2k_s$. Interestingly, $|s^z(k)|^2$ does not have a peak corresponding to $k = 2k_s$. Comparing the peak heights, we can deduce the following inequalities for exponents,

$$x_1 < x_5, x_6 < x_2, x_3, x_4. \quad (86)$$

From the relation $x_l/x_s = x_1/x_2$, we can also obtain

$$x_l < x_s. \quad (87)$$

These observations suggest that the dominant component in the transverse-spin correlation function comes from the first term in Eq. (73) with a wavenumber $\pi \pm k_l$ while the dominant longitudinal-spin correlation comes from the third term in Eq. (76) with a wavenumber $2k_l$.

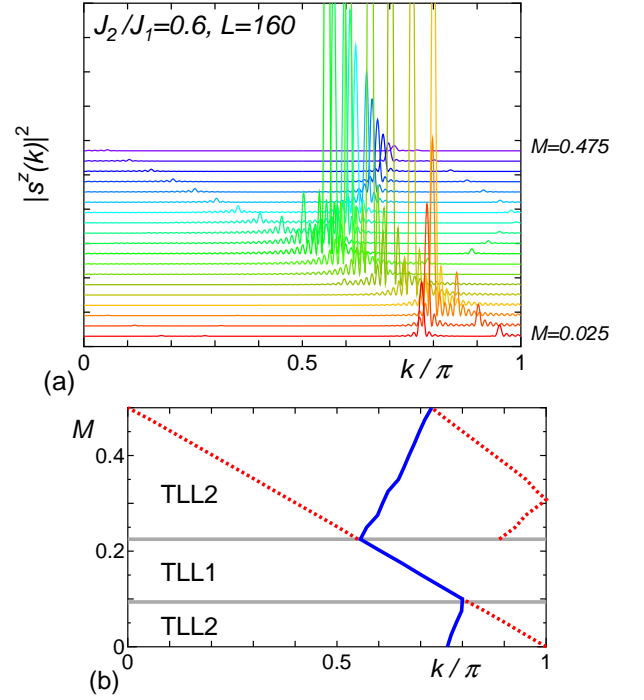


FIG. 16: (Color online) (a) Squared modulus of the Fourier transform of the local spin polarization, $|s^z(k)|^2$, for the antiferromagnetic zigzag ladder with $L = 160$ spins and $J_2/J_1 = 0.6$. (b) M dependence of peak positions of $|s^z(k)|^2$. Solid line represents the highest peak while the dotted lines correspond to the subdominant peaks in TLL2 phase. Gray horizontal lines show phase boundaries.

Figure 17 shows $|s^z(k)|^2$ at $J_2/J_1 = 0.9$. In this case we have the TLL2 phase for $0.35 \lesssim M < 1/2$, the SDW₂ phase for $0.075 \lesssim M \lesssim 0.2$, and the vector chiral phase for $0 < M < 0.05$ and $0.2 \lesssim M \lesssim 0.3$. Characteristics of incommensurate wavenumbers giving rise to the peaks in $|s^z(k)|^2$ in the TLL2 phase are the same as in Fig. 16. In the SDW₂ phase the strong peak is found to be at $k = \pi(1/2 + M)$, in agreement with Eq. (33).

VIII. CONCLUDING REMARKS

By the thorough comparison between numerically obtained correlation functions and asymptotic behaviors derived from low-energy effective theories, we have identified the nature of critical TLL phases that appear in the spin-1/2 J_1 - J_2 AF Heisenberg zigzag ladder under magnetic field. These critical phases consist of three one-component TLL phases (the TLL1, SDW₂, and vector chiral phases) and a two-component TLL phase, the TLL2 phase. From the fitting, we numerically estimated the TLL parameter in one-component TLL phases as a function of J_2/J_1 and the magnetization M . The results allow us to determine the decay exponents of the algebraic spin correlation functions and reveal the dominant

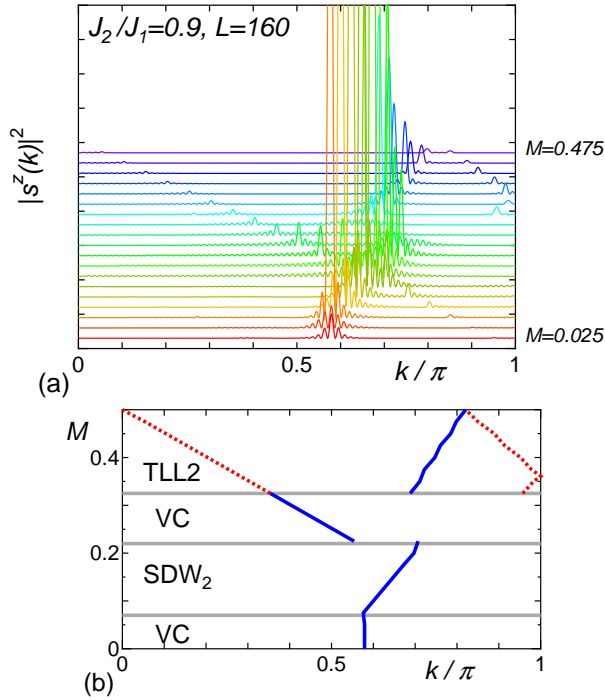


FIG. 17: (Color online) (a) Squared modulus of the Fourier transform of the local spin polarization, $|s^z(k)|^2$, for the antiferromagnetic zigzag ladder with $L = 160$ spins and $J_2/J_1 = 0.9$. (b) M dependence of peak positions of $|s^z(k)|^2$. Solid line represents the highest peak while the dotted lines correspond to the subdominant peaks in TLL2 phase. Gray horizontal lines show phase boundaries.

correlation function in each phase. In addition, we developed an effective theory for the two-component TLL, which reasonably reproduces numerically obtained correlation functions in the TLL2 phase, which appears in two parameter regions in between the TLL1 and vector chiral phases.

One of important implications of our results concerns field-induced phase transitions in quasi-1D compounds, in which weak interchain couplings usually induce a magnetic LRO when the ground state of the pure 1D model is critical.

In the absence of geometrical frustration due to inter-ladder couplings, it is natural to expect that the dominant algebraic correlation in the purely 1D model leads to the magnetic LRO in the real quasi-1D compounds. Based on our results on the correlation functions, we can thus predict that several different magnetic-ordered phases appear in the quasi-1D zigzag ladder compounds; In the parameter regime of the TLL1 phase, we expect a canted antiferromagnetic ordered phase for small J_2/J_1 and an incommensurate longitudinal spin-density wave ordered phase with a wavenumber $Q = \pi(1 \pm 2M)$ for slightly larger J_2/J_1 . The region of the SDW_2 phase

will be replaced by an incommensurate longitudinal spin-density wave ordered phase with $Q_2 = \pm\pi(1/2 + M)$. The vector chiral phase turns into the spiral ordered phase, in which spins perpendicular to the applied field have incommensurate long-range order. This is similar to the classical helical magnetic structure albeit with renormalized pitch and canting angles. For the parameter regime of the TLL2 phase, the system should exhibit the coplanar “fan” phase characterized by the coexistence of incommensurate longitudinal- and transverse-spin LROs. This is consistent with the argument by Ueda and Totsuka;⁷² they showed, using a dilute Bose gas description, that the coplanar fan phase appears near saturation in the quasi-1D system in a wide parameter region around $J_2/J_1 \simeq 1/3$.

Another related quasi-1D system is a spatially anisotropic triangular antiferromagnet, with interchain exchange J' much weaker than the intrachain exchange J . This model was studied recently^{9,88} and the obtained phase diagram shows a resemblance to that of the zigzag ladder. In 1D limit of $J' \ll J$, Starykh and Balents⁹ found a collinear spin-density wave with wave vector $k_x = \pi(1 \pm 2M)$ in intermediate magnetic field regime and a cone phase with spiral transverse order in high magnetic field regime. Kohno¹¹ also found instability to the ordering of incommensurate longitudinal spin-density wave with momentum $k_x = \pi(1 \pm 2M)$ applying weak-coupling analysis to 1D exact solution. If we take a zigzag ladder out of this anisotropic triangular system, the nature of the incommensurate spin-density wave and cone phases, respectively, is essentially the same as that of the SDW_2 and vector chiral phases we showed in the regime of $J_1 \ll J_2$. (Note that the definition of the unit length along chains on the anisotropic triangular lattice is twice larger than that we used in the zigzag ladder.) Transitions from the cone phase to coplanar fan phase with increasing J'/J were also discussed in Ref. 88, which presumably relate to the transitions from the vector chiral phase to the TLL2 phase with increasing J_1/J_2 in the zigzag ladder.

Acknowledgments

It is our pleasure to acknowledge stimulating discussions with Shunsuke Furukawa, Masanori Kohno, Kouichi Okunishi, Shigeki Onoda, Masahiro Sato, and Oleg Starykh. This work was supported in part by Grants-in-Aid for Scientific Research from the Ministry of Education, Culture, Sports, Science and Technology (MEXT) of Japan (Grant No. 17071011, No. 20046016, and No. 21740277) and by the Next Generation Super Computing Project, Nanoscience Program, MEXT, Japan. The numerical calculations were performed in part by using RIKEN Super Combined Cluster (RSCC).

- ¹ P. W. Anderson, Mater. Res. Bull. **8**, 153 (1973).
- ² Y. Shimizu, K. Miyagawa, K. Kanoda, M. Maesato, and G. Saito, Phys. Rev. Lett. **91**, 107001 (2003).
- ³ R. Coldea, D. A. Tennant, A. M. Tsvelik, and Z. Tylczynski, Phys. Rev. Lett. **86**, 1335 (2001).
- ⁴ H. Morita, S. Watanabe, and M. Imada J. Phys. Soc. Jpn. **71**, 2109 (2002).
- ⁵ O. I. Motrunich, Phys. Rev. B **72**, 045105 (2005).
- ⁶ S.-S. Lee and P. A. Lee, Phys. Rev. Lett. **95**, 036403 (2005).
- ⁷ J. Alicea, O. I. Motrunich, and M. P. A. Fisher, Phys. Rev. B **73**, 174430 (2006).
- ⁸ M. Y. Veillette, J. T. Chalker, and R. Coldea, Phys. Rev. B **71**, 214426 (2005).
- ⁹ O. A. Starykh and L. Balents, Phys. Rev. Lett. **98**, 077205 (2007).
- ¹⁰ T. Yoshioka, A. Koga, and N. Kawakami, Phys. Rev. Lett. **103**, 036401 (2009).
- ¹¹ M. Kohno, Phys. Rev. Lett. **103**, 197203 (2009).
- ¹² D. B. Brown, J. A. Donner, J. W. Hall, S. R. Wilson, R. B. Wilson, D. J. Hodgson, and W. E. Hatfield, Inorg. Chem. **18**, 2635 (1979).
- ¹³ M. Hagiwara, Y. Narumi, K. Kindo, N. Maeshima, K. Okunishi, T. Sakai, and M. Takahashi, Physica B **294-295**, 83 (2001).
- ¹⁴ N. Maeshima, M. Hagiwara, Y. Narumi, K. Kindo, T. C. Kobayashi, and K. Okunishi, J. Phys.: Condens. Matter **15**, 3607 (2003).
- ¹⁵ For a list of the zigzag-ladder materials, see, for example, Table I in M. Hase, H. Kuroe, K. Ozawa, O. Suzuki, H. Kitazawa, G. Kido, and T. Sekine, Phys. Rev. B **70**, 104426 (2004).
- ¹⁶ M. Enderle, C. Mukherjee, B. Fåk, R. K. Kremer, J.-M. Broto, H. Rosner, S.-L. Drechsler, J. Richter, J. Malek, A. Prokofiev, W. Assmus, S. Pujol, J.-L. Raggazzoni, H. Rakoto, M. Rheinstädter, and H. M. Rønnow, Europhys. Lett. **70**, 237 (2005).
- ¹⁷ M. G. Banks, F. Heidrich-Meisner, A. Honecker, H. Rakoto, J.-M. Broto, and R. K. Kremer, J. Phys.: Condens. Matter **19**, 145227 (2007).
- ¹⁸ N. Büttgen, H.-A. Krug von Nidda, L. E. Svistov, L. A. Prozorova, A. Prokofiev, and W. Assmus, Phys. Rev. B **76**, 014440 (2007).
- ¹⁹ Y. Naito, K. Sato, Y. Yasui, Y. Kobayashi, Y. Kobayashi, and M. Sato, J. Phys. Soc. Jpn. **76**, 023708 (2007); Y. Yasui, Y. Naito, K. Sato, T. Moyoshi, M. Sato, and K. Kakurai, *ibid.* **77**, 023712 (2008).
- ²⁰ F. Schrettle, S. Krohns, P. Lunkenheimer, J. Hemberger, N. Büttgen, H.-A. Krug von Nidda, A. V. Prokofiev, and A. Loidl, Phys. Rev. B **77**, 144101 (2008).
- ²¹ K. Okunishi and T. Tonegawa, J. Phys. Soc. Jpn. **72**, 479 (2003).
- ²² T. Hikihara, L. Kecke, T. Momoi, and A. Furusaki, Phys. Rev. B **78**, 144404 (2008).
- ²³ J. Sudan, A. Läuscher, and A. M. Läuchli, Phys. Rev. B **80**, 140402(R) (2009).
- ²⁴ F. Heidrich-Meisner, I. P. McCulloch, and A. K. Kolezhuk, Phys. Rev. B **80**, 144417 (2009).
- ²⁵ C. K. Majumdar and D. K. Ghosh, J. Math. Phys. **10**, 1388 (1969).
- ²⁶ C. K. Majumdar and D. K. Ghosh, J. Math. Phys. **10**, 1399 (1969).
- ²⁷ F. D. M. Haldane, Phys. Rev. B **25**, 4925 (1982).
- ²⁸ S. R. White and I. Affleck, Phys. Rev. B **54**, 9862 (1996).
- ²⁹ R. Jullien and F. D. M. Haldane, Bull. Am. Phys. Soc. **28**, 344 (1983).
- ³⁰ K. Okamoto and K. Nomura, Phys. Lett. A **169**, 433 (1992).
- ³¹ S. Eggert, Phys. Rev. B **54**, R9612 (1996).
- ³² A. A. Nersisyan, A. O. Gogolin, and F. H. L. Eßler, Phys. Rev. Lett. **81**, 910 (1998).
- ³³ M. Kaburagi, H. Kawamura, and T. Hikihara, J. Phys. Soc. Jpn. **68**, 3185 (1999).
- ³⁴ T. Hikihara, M. Kaburagi, and H. Kawamura, Phys. Rev. B **63**, 174430 (2001).
- ³⁵ K. Okunishi, Y. Hieida, and Y. Akutsu, Phys. Rev. B **60**, R6953 (1999).
- ³⁶ K. Okunishi and T. Tonegawa, Phys. Rev. B **68**, 224422 (2003).
- ³⁷ T. Tonegawa, K. Okamoto, K. Okunishi, K. Nomura, and M. Kaburagi, Physica B **346-347**, 50 (2004).
- ³⁸ T. Hikihara, M. Kaburagi, H. Kawamura and T. Tonegawa, J. Phys. Soc. Jpn. **69**, 259 (2000).
- ³⁹ T. Hikihara, J. Phys. Soc. Jpn. **71**, 319 (2002).
- ⁴⁰ T. Momoi, J. Stat. Phys. **85**, 193 (1996).
- ⁴¹ A. Kolezhuk and T. Vekua, Phys. Rev. B **72**, 094424 (2005).
- ⁴² I. P. McCulloch, R. Kube, M. Kurz, A. Kleine, U. Schollwöck, and A. K. Kolezhuk, Phys. Rev. B **77**, 094404 (2008).
- ⁴³ K. Okunishi, J. Phys. Soc. Jpn. **77**, 114004 (2008).
- ⁴⁴ S. R. White, Phys. Rev. Lett. **69**, 2863 (1992).
- ⁴⁵ S. R. White, Phys. Rev. B **48**, 10345 (1993).
- ⁴⁶ T. Giamarchi, *Quantum Physics in One Dimension* (Clarendon Press, Oxford, 2004).
- ⁴⁷ M. Sato, T. Momoi, and A. Furusaki, Phys. Rev. B **79**, 060406(R) (2009).
- ⁴⁸ A. V. Chubukov, Phys. Rev. B **44**, 4693 (1991).
- ⁴⁹ D. C. Cabra, A. Honecker, and P. Pujol, Eur. Phys. J. B **13**, 55 (2000).
- ⁵⁰ F. Heidrich-Meisner, A. Honecker, and T. Vekua, Phys. Rev. B **74**, 020403(R) (2006).
- ⁵¹ L. Kecke, T. Momoi, and A. Furusaki, Phys. Rev. B **76**, 060407(R) (2007).
- ⁵² T. Vekua, A. Honecker, H.-J. Mikeska, and F. Heidrich-Meisner, Phys. Rev. B **76**, 174420 (2007).
- ⁵³ A. M. Läuchli, J. Sudan, and A. Läuscher, J. Phys: Conf. Series, **145**, 012057 (2009).
- ⁵⁴ T. Hikihara and A. Furusaki, Phys. Rev. B **58**, R583 (1998).
- ⁵⁵ T. Hikihara and A. Furusaki, Phys. Rev. B **63**, 134438 (2001).
- ⁵⁶ T. Hikihara and A. Furusaki, Phys. Rev. B **69**, 064427 (2004).
- ⁵⁷ H. J. Schulz, Phys. Rev. B **22**, 5274 (1980).
- ⁵⁸ R. Chitra and T. Giamarchi, Phys. Rev. B **55**, 5816 (1997).
- ⁵⁹ N. M. Bogoliubov, A. G. Izergin, and V. E. Korepin, Nucl. Phys. B **275**, 687 (1986).
- ⁶⁰ D. C. Cabra, A. Honecker, and P. Pujol, Phys. Rev. B **58**, 6241 (1998).
- ⁶¹ G. Fáth, Phys. Rev. B **68**, 134445 (2003).
- ⁶² C. Gerhardt, A. Fledderjohann, E. Aysal, K.-H. Mütter, J. F. Audet, and H. Kröger, J. Phys.: Condens. Matter **9**,

- 3435 (1997).
- ⁶³ M. Usami and S. Suga, Phys. Lett. A **240**, 85 (1998).
- ⁶⁴ N. Haga and S. Suga, J. Phys. Soc. Jpn. **69**, 2431 (2000).
- ⁶⁵ T. Suzuki and S. Suga, Phys. Rev. B **70**, 054419 (2004).
- ⁶⁶ N. Maeshima, K. Okunishi, K. Okamoto, and T. Sakai, Phys. Rev. Lett. **93**, 127203 (2004).
- ⁶⁷ P. Lecheminant and E. Orignac, Phys. Rev. B **69**, 174409 (2004).
- ⁶⁸ K. Hida and I. Affleck, J. Phys. Soc. Jpn. **74**, 1849 (2005).
- ⁶⁹ Note that the definition of the ϕ (θ) field in the present paper differs from that in Refs. 67 and 68 by a factor $1/\sqrt{2}$ ($\sqrt{2}$) and $1/\sqrt{2\pi}$ ($\sqrt{2\pi}$), respectively.
- ⁷⁰ In Ref. 21, the SDW₂ phase was termed even-odd phase, while we call it the SDW₂ phase after its physical properties (see Sec. IV).
- ⁷¹ T. Hikihara, A. Furusaki, and K. A. Matveev, Phys. Rev. B **72**, 035301 (2005).
- ⁷² H. T. Ueda and K. Totsuka, Phys. Rev. B **80**, 014417 (2009).
- ⁷³ F. D. M. Haldane, Phys. Rev. Lett. **47**, 1840 (1981).
- ⁷⁴ B. S. Shastry and B. Sutherland, Phys. Rev. Lett. **47**, 964 (1981).
- ⁷⁵ S. Brehmer, A. K. Kolezhuk, H.-J. Mikeska, and U. Neugebauer, J. Phys.: Condens. Matter **10**, 1103 (1998).
- ⁷⁶ K. Okunishi and N. Maeshima, Phys. Rev. B **64**, 212406 (2001).
- ⁷⁷ H. Frahm and C. Rödenbeck, J. Phys. A: Math. Gen. **30**, 4467 (1997).
- ⁷⁸ H. Frahm and C. Rödenbeck, Eur. Phys. J. B **10**, 409 (1999).
- ⁷⁹ V. L. Pokrovsky and A. L. Talapov, Phys. Rev. Lett. **42**, 65 (1979).
- ⁸⁰ P. W. Anderson, *Basic Notions of Condensed Matter Physics* (Addison-Wesley, Reading, 1997).
- ⁸¹ M. A. Cazalilla and A. F. Ho, Phys. Rev. Lett. **91**, 150403 (2003).
- ⁸² A. K. Kolezhuk, Phys. Rev. A **81**, 013601 (2010).
- ⁸³ Kun Yang, Phys. Rev. Lett. **93**, 066401 (2004).
- ⁸⁴ C. Holzhey, F. Larsen, and F. Wilczek, Nucl. Phys. **B424**, 443 (1994).
- ⁸⁵ P. Calabrese and J. Cardy, J. Stat. Mech.: Theory Exp. **(2004)** P06002.
- ⁸⁶ G. Vidal, J. I. Latorre, E. Rico, and A. Kitaev, Phys. Rev. Lett. **90**, 227902 (2003).
- ⁸⁷ D. N. Sheng, O. I. Motrunich, and M. P. A. Fisher, Phys. Rev. B **79**, 205112 (2009).
- ⁸⁸ J. Alicea, A. V. Chubukov, and O. A. Starykh, Phys. Rev. Lett. **102**, 137201 (2009).